Figure 1 Genomic structure and domain organization of human ADAMTS13 and nonsynonymous mutations identified in patients with congenital thrombotic thrombocytopenic purpura

Missense mutations are indicated by black spades. Nonsense mutations, insertion/deletion mutations, and splice site mutations are shown by hearts, clubs, and diamonds, respectively. The P475S mutation commonly observed in the Japanese population and the A insertion at nucleotide number 4143 found in multiple European populations are shown. S, signal peptide; P, propeptide; Dis, disintegrin-like domain; T (numbered 1–8), thrombospondin type 1 motifs; CUB, complement components C1r/C1s, Uegf (epidermal growth factor-related sea urchin protein), and bone morphogenetic protein-1; Cys, cysteine-rich domain.

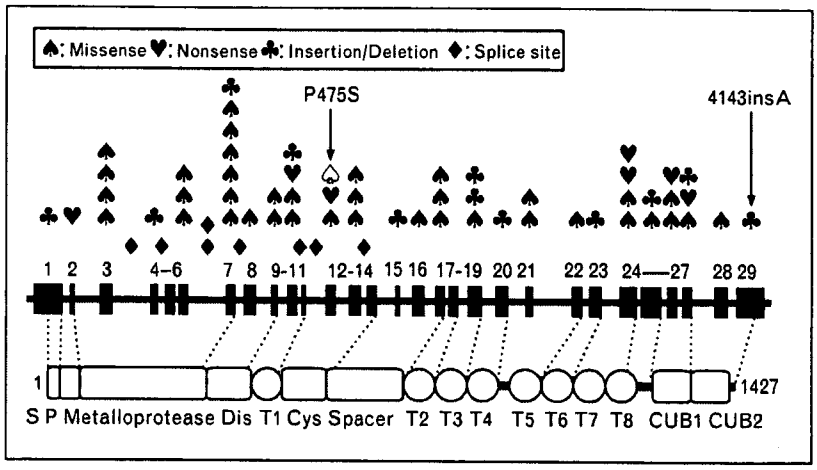

More than 60 different mutations of the ADAMTS13 gene have been reported [6,17–19,20*,21]. More than 50% are missense mutations, as well as frame-shift mutations such as insertions and deletions, and nonsense mutations and splice-site mutations. These mutations are distributed throughout the various domains of ADAMTS13 (Fig. 1). The correlation of genotype and protease activity in some of these mutations has been examined by expression analysis in vitro [18,20*,21]. Most of the mutations have been identified in a single family but there are at least six recurrent mutations in unrelated patients. Among them, the 4143insA mutation has been identified as a genetic background for TTP in multiple families and is frequent among patients with congenital ADAMTS13 deficiency in Northern and Central European countries [22**]. Interestingly, several missense mutations can interact and alter the phenotype of ADAMTS13 deficiency [23**].

There are at least nine missense polymorphisms in the ADAMTS13 gene. The Q448E mutation was shown not to affect the protease activity, whereas the P475S mutation decreased the activity [18]. This mutation is present in the Asian population but not in the white population [19,24,25]. It has been shown not to be a genetic risk factor for deep-vein thrombosis [26*].

Information regarding the wide variation of phenotypes in TTP patients with congenital ADAMTS13 deficiency has accumulated. Most patients with congenital ADAMTS13 deficiency had their first episode as newborn babies or in early infancy [10*]. After this period, the clinical manifestations of congenital ADAMTS13 deficiency vary from patient to patient, and patients are often incorrectly diagnosed with idiopathic thrombocytopenic purpura or Evans' syndrome during childhood. Seven women with congenital ADAMTS13 deficiency who exhibited TTP at 5–6 months of pregnancy have been reported [27].

The factor V Leiden mutation is a well characterized and the most prevalent genetic risk factor for venous thrombosis. A previous study suggested that the factor V Leiden mutation may be a pathogenic risk factor in patients with thrombotic microangiopathy who have normal ADAMTS13 activity [28]. A recent study did not support the link between the factor V Leiden mutation and thrombotic microangiopathy [29].

Hemolytic uremic syndrome (HUS) is a thrombotic microangiopathy with manifestations of hemolytic anemia, thrombocytopenia, and renal impairment [1,8*,9**,30]. In most cases, typical HUS is triggered by Shiga toxin-producing Escherichia coli and manifests diarrhea (D+ HUS). Atypical non-Shiga toxin-associated HUS is not associated with diarrhea (D- HUS), and deficiencies of complement factor H, membrane cofactor protein, and complement factor I have been reported in such atypical HUS [9**,31].

Epitopes of ADAMTS13 autoantibodies

Inhibitory autoantibodies for ADAMTS13 cause a deficiency of ADAMTS13 among patients with autoimmune TTP [3**,8**]. The prevalence of ADAMTS13 deficiency among patients with TTP varies from 13 to 100% depending on the criteria of the study. TTP may develop within 2–6 weeks after the antiplatelet agent ticlopidine is administered. TTP may develop in patients with HIV infection. No other apparent etiologies of inhibitory autoantibodies have been identified.

Several studies using recombinant ADAMTS13 and its truncated forms have identified the epitopes of

autoantibodies in patients with TTP. Many inhibitory autoantibodies recognized the spacer domain as the target epitope [32–34,35•]. Some reacted with the C-terminal CUB domains and the first thrombospondin type-1 (TSP-1) repeat [33]. Multiple B-cell clones producing antibodies directed against the spacer domain have been reported [36].

Assays of ADAMTS13 activity

ADAMTS13 assays such as multimer analysis by SDS/agarose-gel electrophoresis and residual collagen-binding analysis have been utilized for plasma ADAMTS13 activity in thrombotic microangiopathies and other pathophysiological conditions [2,4,6]. These assays quantify ADAMTS13 activity by measuring residual VWF multimers or their activity, suggesting that more accurate and simpler assays are in demand.

New assays using VWF73 peptide as the ADAMTS13 substrate

In 2004, we identified a 73-amino acid sequence spanning residues D1596–R1668 of the VWF A2 domain, VWF73, as the minimum region for ADAMTS13 cleavage [37]. A shorter peptide, VWF64, from D1596 to R1659, was not a good substrate for ADAMTS13. Since the development of VWF73 as the substrate for ADAMTS13, several new assays based on the VWF73 sequence have been developed [37–39,40•–43•]. So far, seven assays have been published for the VWF73-based measurements of ADAMTS13 activity. The characteristics of these assays are summarized in Table 1 [37–39,40•–43•]. The assays have the advantages of being simple, rapid, accurate, and quantitative. They do not require denaturing conditions; therefore, the incubation time of the substrates and plasma samples is reduced to less than 1 h. They give rise to quantitative measures. In addition, most of the assays are compatible with the 96-well microplates that clinical-laboratory workers are familiar with, so they have the potential to be widely used in clinical settings.

Of the seven assays, FRETS-VWF73, a fluorogenic substrate for ADAMTS13, is well characterized. The advantage of using FRETS-VWF73 is that the ADAMTS13 activity can be determined by the initial velocity of the increase in fluorescence. Therefore, the assay is highly quantitative. ADAMTS13 cleaves VWF with a $K_m$app of 3.7 • 1.4 mg/ml or 15 nM in VWF subunits, which is comparable with the plasma VWF concentration of 5–10 mg/ml, and with a value for k_{cat} of • 0.83 min^{-1} [44•]. ADAMTS13 cleaves FRETS-VWF73 with a $K_m$app of 3.2 • 1.1 mM and a k_{cat} of • 58 min^{-1}. Thus, the affinity of ADAMTS13 to FRETS-VWF73 was decreased • 200-fold compared with VWF, but the catalytic efficiency was • 70-fold greater than VWF. Therefore, ADAMTS13 cleaves VWF and FRETS-VWF73 with roughly comparable catalytic efficiencies of 55 and 18 $mM^{-1} min^{-1}$, respectively [44•].

FRETS-VWF73 was evaluated by three different research groups [45–47]. Although the definitive evaluation remains to be determined in a large cohort of patients diagnosed with acquired or congenital TTP, ADAMTS13 activity determined by FRETS-VWF73 assay was in good accordance with that measured by conventional assays. FRETS-VWF73 is now commercially available (Table 2).

There may be limitations of the VWF73-based ADAMTS13 assays. VWF73, a small fragment of the A2 domain of VWF, may lack additional sites on VWF that interact with ADAMTS13. The A1 domain of VWF binds cofactors such as platelet glycoprotein Ib and heparin to regulate cleavage [48], and the A3 domain may be a docking site for ADAMTS13 [49]. VWF73 lacks

Table 1 VWF73-based ADAMTS13 activity assays

Substrate	Principle	Reference
GST–VWF73 fusion protein with the C-terminal 6• His tag	Western-blot detection using anti-GST antibody	[37]
FRETS-VWF73, synthetic VWF73 peptide with a fluorophore at the P7 position and a quencher at the $P5^{I}$ position	Fluorescence resonance energy transfer, initial-velocity method	[39]
Immobilized GST–VWF73 fusion protein with the C-terminal 6• His tag	Enzyme immunoassay, the amount of 6• His remaining was assayed with anti-6• His IgG conjugated with HRP, end point method	[38]
Immobilized His- and biotin-labeled VWF73 conjugated with HRP	Enzyme-linked assay, endpoint method	[40•]
Immobilized GST–VWF73 fusion protein with the C-terminal 6• His tag	Mass-spectrometry analysis of the products, endpoint method	[41•]
Immobilized GST–VWF73 fusion protein with the C-terminal 6• His tag	Enzyme immunoassay, the amount of products were assayed with anti-N10 mAbs conjugated with HRP, endpoint method	[42•]
Recombinant 6• His-tagged VWF73 peptide labeled with fluorescein at both the P7 and $P6^{I}$ positions	Fluorescence resonance energy transfer, initial-velocity method	[43•]

GST, glutathione-S-transferase; HRP, horseradish peroxidase; mAb, monoclonal antibody; VWF73, 73 amino acid residues of von Willebrand factor (VWF) from D1596 to R1668.

Table 2 Commercially available kits for assaying ADAMTS13 activity and antigen

Kit	Maker/supplier	Objectives	Time
FRETS-VWF73	Peptide Institute, Peptides International	Activity	1 h
ATS-13 ADAMTS-13 Activity	GTI	Activity	30 min
ADAMTS13 ELISA kit	Mitsubishi Kagaku Iatron	Antigen	3.5 h
ADAMTS13 activity ELISA kit	KAINOS LABORATORIES	Activity	3.5 h
TECHNOZYM ADAMTS-13	Technoclone GmbH	Activity/antigen	2.5 h/4 h
TECHNOZYM ADAMTS-13 INH	Technoclone GmbH	Autoantibody	2.5 h
ACTIFLUOR ADAMTS13 Activity Assay kit	American Diagnostica	Activity	
IMUBIND ADAMTS13 ELISA	American Diagnostica	Antigen	5 h
IMUBIND ADAMTS13/fXI Complex ELISA	American Diagnostica	ADAMTS13/FXI complex	4 h
IMUBIND ADAMTS13 Autoantibody ELISA	American Diagnostica	Autoantibody	4 h

these domains. Therefore, if enzyme defects in patients with TTP affect the ADAMTS13-binding site for these domains, cleavage of VWF73 will not reflect these defects.

Measurements of ADAMTS13 autoantibodies

Autoantibodies neutralizing ADAMTS13 activity are a major cause of acquired TTP. The presence or absence of inhibitory autoantibodies is important in discriminating acquired from congenital TTP. An inhibitor assay is generally carried out using mixtures of heat-inactivated plasma from patients and normal plasma at a 1:1 dilution or several dilutions. Assays for ADAMTS13 activity so far developed, including VWF73-based assays, are compatible for the inhibitor assay. It should be noted that nonneutralizing autoantibodies may reduce the circulating ADAMTS13 levels by antibody-mediated clearance.

ELISA has been developed to detect autoantibodies against ADAMTS13. In this process, immobilized ADAMTS13 in the plate wells captures both inhibitory and noninhibitory autoantibodies in plasma samples; then secondary detection antibodies, such as goat antihuman IgG or IgM antibodies labeled with horseradish peroxidase, are added and the levels of ADAMTS13-binding IgGs are determined [50]. Using this assay, low titers of IgG antibodies were detected in four out of 111 healthy control donors who lacked anti-ADAMTS13 inhibitory activity by inhibitor assays. IgG autoantibodies were found in 97% of untreated patients with acute acquired thrombotic microangiopathies who had plasma ADAMTS13 activity levels below 10% [51]. This assay was more sensitive than the standard functional inhibitor assay for detecting autoantibodies against ADAMTS13. The ELISA kit utilizing this principle is now commercially available (Table 2), and has been validated to be useful [52].

Antigen assays for plasma ADAMTS13

ELISA for measuring plasma ADAMTS13 antigen levels has also been developed by several research groups. ADAMTS13 antigen ELISA kits are also commercially available (Table 2).

Healthy plasma ADAMTS13 levels

The ELISA assay to detect plasma ADAMTS13 levels can estimate the plasma ADAMTS13 concentration when the ADAMTS13 standard can be obtained from recombinant full-length ADAMTS13 protein. The ADAMTS13 antigen concentration in normal human plasma pooled from white donors was 1.03• 0.15 mg/ml of plasma [53•]. Interestingly, normal Chinese donors have significantly lower antigen levels (0.62• 0.13 mg/ml). In another study of 99 healthy Austrian donors, the median plasma ADAMTS13 level was 1.08 mg/ml using recombinant ADAMTS13 as the standard [54•]. The plasma ADAMTS13 level in Japanese donors was reported to be 0.82• 0.15 and 0.70• 0.13 mg/ml using two different ELISA systems when recombinant ADAMTS13 was used as the standard [55•].

Phenotype of mice lacking Adamts13 gene

The mouse is a promising animal model for seeking genetic or environmental susceptibility factor(s) for a certain disease phenotype. Two types of mouse Adamts13 cDNA have been isolated and characterized [56]. cDNA isolated from the 129/Sv strain showed a domain organization identical to the human one. The other cDNA lacked the C-terminal two TSP-1 motifs and two CUB domains due to the insertion of an intracisternal A particle retrotransposon in intron 23, which creates a premature stop codon. Both recombinant proteins showed VWF-cleaving activity in vitro.

Mice lacking the Adamts13 gene have been recently developed by us and another group [57,58••,59••]. We generated mice lacking the Adamts13 gene by replacing exons 3–6 encoding the catalytic domain by a neomycin-resistant cassette and analyzed phenotypes on a 129/Sv genetic background of the ADAMTS13-deficient mice [58••]. The ADAMTS13-deficient mice were born in the expected Mendelian distribution. Plasma from homozygous mice showed no ADAMTS13 activity. The mice were viable and fertile. Hematologic and histologic examinations failed to detect any evidence of thrombocytopenia, hemolytic anemia, or microvascular thrombosis. However, ULVWF multimers were observed in the plasma of homozygotes. Thrombus formation on immobilized

collagen under flow was significantly elevated in homozygotes in comparison with wild-type mice. Thrombocytopenia was more severely induced in homozygotes than in wild-type mice after intravenous injection of a mixture of collagen and epinephrine. Therefore, a complete lack of ADAMTS13 in mice caused a prothrombotic state, but it alone was not sufficient to cause TTP. Factors in addition to ADAMTS13 deficiency may be necessary for development of TTP.

Mice lacking the Adamts13 gene have also been generated with replacement of exons 1–6 by a neomycin cassette [57]. The ADAMTS13-deficient mice were born in the expected Mendelian distribution and homozygous mice were viable and fertile. When the VWF multimer analysis was examined in the ADAMTS13-deficient mice on a mixed-strain C57BL/6J and 129X1/SvJ genetic background, the multimers of wild-type mice and ADAMTS13-deficient mice were indistinguishable. However, the ADAMTS13-deficient mice, after two generations of backcrossing to the CASA/Rk strain (a mouse strain with elevated plasma VWF), showed ULVWF multimers compared with wild-type littermates. Mice with a mixed CASA/Rk background showed a significant decrease in platelet count and a fraction of the deficient mice exhibited severe thrombocytopenia and significantly decreased survival compared with wild-type or heterozygous controls. These mice showed a TTP-like phenotype such as severe microangiopathic changes in the peripheral blood and VWF-rich and fibrin-poor hyaline thrombi in the small vessels. Deficient mice showed prolongation of VWF-mediated platelet-endothelial interactions, indicating that ADAMTS13 regulates VWF-mediated platelet adhesion in vivo. When Shiga toxin was infused intravenously, TTP-like symptoms were observed in ADAMTS13-deficient mice with a mixed CASA/Rk background, but not in mice with a mixed C57BL/6J background. Shiga toxin is known to induce HUS through endothelial dysfunction. Thus, TTP can be induced in ADAMTS13-deficient mice by agents causing endothelial dysfunction. This strain-specific difference of TTP pathogenesis in mice may indicate the contribution of additional genetic factors.

Further characterizations of events in vivo in ADAMTS13-deficient mice on a mixed-strain C57BL/6J and 129X1/SvJ genetic background have been examined [59•]. When the microvenule endothelium in ADAMTS13-deficient mice was activated with calcium ionophore, ULVWF multimers were secreted from Weibel–Palade body, and platelet aggregation resulting in spontaneous thrombus formation was observed using intravital microscopy. In wild-type littermates, platelet strings and very small aggregation could be seen attached to the endothelium, but thrombi did not form. A ferric chloride injury model on arterioles exhibited that ADAMTS13 downregulates both platelet adhesion to the exposed subendothelium and thrombus formation. Infusion of recombinant ADAMTS13 into ADAMTS13-deficient or wild-type mice inhibited similar thrombus growth. These findings revealed that ADAMTS13 is a natural anticoagulant.

Conclusion

A highly accurate and quantitative assay method for measuring ADAMTS13 activity has been developed. These assays are now commercially available and will be widely utilized for a clinical diagnosis in patients with microangiopathy to discriminate TTP from HUS or other thrombocytopenia. Mice lacking the Adamts13 gene were viable and fertile. They did not show the TTP-like phenotype such as spontaneous thrombocytopenia, but intensive analyses revealed that they were prothrombotic. They are useful models to reveal how ADAMTS13 deficiency interacts with other genetic and environmental factors.

Acknowledgements

We thank Dr Tomoko Ono for providing Table 2. This study was supported in part by the Program for Promotion of Fundamental Studies in Health Sciences of the National Institute of Biomedical Innovation (NIBIO) of Japan, and a grant-in-aid from the Ministry of Health, Labor, and Welfare of Japan and the Ministry of Education, Culture, Sports, Science, and Technology of Japan.

References and recommended reading

Papers of particular interest, published within the annual period of review, have been highlighted as:

- • of special interest
- •• of outstanding interest

Additional references related to this topic can also be found in the Current World Literature section in this issue (p. 296).

1 Moake JL. Thrombotic microangiopathies. N Engl J Med 2002; 347:589–600.

2 Sadler JE, Moake JL, Miyata T, George JN. Recent advances in thrombotic thrombocytopenic purpura. Hematology Am Soc Hematol Edu Program 2004; 407–423.

3 •• Sadler JE. Thrombotic thrombocytopenic purpura: a moving target. Hematology Am Soc Hematol Edu Program 2006; 415–420.
This review integrates the current knowledge about ADAMTS13 into a model of TTP.

4 Miyata T, Kokame K, Banno F. Measurement of ADAMTS13 activity and inhibitors. Curr Opin Hematol 2005; 12:384–389.

5 Levy GG, Motto DG, Ginsburg D. ADAMTS13 turns 3. Blood 2005; 106: 11–17.

6 Shelat SG, Ai J, Zheng XL. Molecular biology of ADAMTS13 and diagnostic utility of ADAMTS13 proteolytic activity and inhibitor assays. Semin Thromb Hemost 2005; 31:659–672.

7 • Bowen DJ, Collins PW. Insights into von Willebrand factor proteolysis: clinical implications. Br J Haematol 2006; 133:457–467.
This review summarizes the clinical implications of VWF proteolysis, especially in the ABO blood group and VWF polymorphism.

8 •• Tsai HM. Current concepts in thrombotic thrombocytopenic purpura. Annu Rev Med 2006; 57:419–436.
This review summarizes recent advances in autoimmune TTP and hereditary TTP.

9 •• Tsai HM. The molecular biology of thrombotic microangiopathy. Kidney Int 2006; 70:16–23.
This review deals with TTP and atypical HUS.

10 • Loirat C, Veyradier A, Girma JP, et al. Thrombotic thrombocytopenic purpura associated with von Willebrand factor-cleaving protease (ADAMTS13) deficiency in children. Semin Thromb Hemost 2006; 32:90–97.
The review deals with children with TTP.

11 Uemura M, Tatsumi K, Matsumoto M, et al. Localization of ADAMTS13 to the stellate cells of human liver. Blood 2005; 106:922–924.

12 Zhou W, Inada M, Lee TP, et al. ADAMTS13 is expressed in hepatic stellate cells. Lab Invest 2005; 85:780–788.

13 Suzuki M, Murata M, Matsubara Y, et al. Detection of von Willebrand factor-cleaving protease (ADAMTS-13) in human platelets. Biochem Biophys Res Commun 2004; 313:212–216.

14 Liu L, Choi H, Bernardo A, et al. Platelet-derived VWF-cleaving metalloprotease ADAMTS-13. J Thromb Haemost 2005; 3:2536–2544.

15 • Turner N, Nolasco L, Tao Z, et al. Human endothelial cells synthesize and release ADAMTS-13. J Thromb Haemost 2006; 4:1396–1404.
The authors reported human endothelial cells as ADAMTS13-producing cells.

16 •• Shang D, Zheng XW, Niiya M, Zheng XL. Apical sorting of ADAMTS13 in vascular endothelial cells and Madin-Darby canine kidney cells depends on the CUB domains and their association with lipid rafts. Blood 2006; 108: 2207–2215.
This study identified C-terminal CUB domains as the apical sorting signal of the ADAMTS13 molecule.

17 Levy GG, Nichols WC, Lian EC, et al. Mutations in a member of the ADAMTS gene family cause thrombotic thrombocytopenic purpura. Nature 2001; 413:488–494.

18 Kokame K, Matsumoto M, Soejima K, et al. Mutations and common polymorphisms in ADAMTS13 gene responsible for von Willebrand factor-cleaving protease activity. Proc Natl Acad Sci USA 2002; 99:11902–11907.

19 Kokame K, Miyata T. Genetic defects leading to hereditary thrombotic thrombocytopenic purpura. Semin Hematol 2004; 41:34–40.

20 • Donadelli R, Banterla F, Galbusera M, et al. In-vitro and in-vivo consequences of mutations in the von Willebrand factor cleaving protease ADAMTS13 in thrombotic thrombocytopenic purpura. Thromb Haemost 2006; 96:454–464.
The authors reported ADAMTS13 mutations and polymorphisms on behalf of the International Registry of Recurrent and Familial HUS/TTP.

21 Peyvandi F, Lavoretano S, Palla R, et al. Mechanisms of the interaction between two ADAMTS13 gene mutations leading to severe deficiency of enzymatic activity. Hum Mutat 2006; 27:330–336.

22 •• Schneppenheim R, Kremer Hovinga JA, Becker T, et al. A common origin of the 4143insA ADAMTS13 mutation. Thromb Haemost 2006; 96:3–6.
The authors identified the 4143insA mutation in the ADAMTS13 gene as a common origin for ADAMTS13 deficiency in European lineages.

23 •• Plaimauer B, Fuhrmann J, Mohr G, et al. Modulation of ADAMTS13 secretion and specific activity by a combination of common amino acid polymorphisms and a missense mutation. Blood 2006; 107:118–125.
Two patients with congenital TTP carried five missense mutations that can interact with each other, thereby altering the phenotype of ADAMTS13 deficiency.

24 Ruan C, Dai L, Su J, et al. The frequency of P475S polymorphism in von Willebrand factor-cleaving protease in the Chinese population and its relevance to arterial thrombotic disorders. Thromb Haemost 2004; 91: 1257–1258.

25 Bongers TN, De Maat MP, Dippel DW, et al. Absence of Pro475Ser polymorphism in ADAMTS-13 in Caucasians. J Thromb Haemost 2005; 3: 805.

26 • Kimura R, Honda S, Kawasaki T, et al. Protein S-K196E mutation as a genetic risk factor for deep vein thrombosis in Japanese patients. Blood 2006; 107:1737–1738.
The P475S mutation in ADAMTS13 was not a risk factor for deep-vein thrombosis.

27 Matsuyama T, Matsumoto M, Kato S, et al. Upshaw-Schulman syndrome: a masqueraded thrombocytopenia during pregnancy. Blood 2005; 106: abstract no. 2644.

28 Raife TJ, Lentz SR, Atkinson BS, et al. Factor V Leiden: a genetic risk factor for thrombotic microangiopathy in patients with normal von Willebrand factor-cleaving protease activity. Blood 2002; 99:437–442.

29 Krieg S, Studt JD, Sulzer I, et al. Is factor V Leiden a risk factor for thrombotic microangiopathies without severe ADAMTS 13 deficiency? Thromb Haemost 2005; 94:1186–1189.

30 Shibagaki Y, Fujita T. Thrombotic microangiopathy in malignant hypertension and hemolytic uremic syndrome (HUS)/thrombotic thrombocytopenic purpura (TTP): can we differentiate one from the other? Hypertens Res 2005; 28:89–95.

31 Caprioli J, Noris M, Brioschi S, et al. Genetics of HUS: the impact of MCP, CFH, and IF mutations on clinical presentation, response to treatment, and outcome. Blood 2006; 108:1267–1279.

32 Soejima K, Matsumoto M, Kokame K, et al. ADAMTS-13 cysteine-rich/spacer domains are functionally essential for von Willebrand factor cleavage. Blood 2003; 102:3232–3237.

33 Klaus C, Plaimauer B, Studt JD, et al. Epitope mapping of ADAMTS13 autoantibodies in acquired thrombotic thrombocytopenic purpura. Blood 2004; 103:4514–4519.

34 Luken BM, Turenhout EA, Hulstein JJ, et al. The spacer domain of ADAMTS13 contains a major binding site for antibodies in patients with thrombotic thrombocytopenic purpura. Thromb Haemost 2005; 93:267–274.

35 • Luken BM, Turenhout EA, Kaijen PH, et al. Amino acid regions 572-579 and 657-666 of the spacer domain of ADAMTS13 provide a common antigenic core required for binding of antibodies in patients with acquired TTP. Thromb Haemost 2006; 96:295–301.
The authors reported the spacer domain of ADAMTS13 to be the autoantibody target.

36 Luken BM, Kaijen PH, Turenhout EA, et al. Multiple B-cell clones producing antibodies directed to the spacer and disintegrin/thrombospondin type-1 repeat 1 (TSP1) of ADAMTS13 in a patient with acquired thrombotic thrombocytopenic purpura. J Thromb Haemost 2006; 4:2355–2364.

37 Kokame K, Matsumoto M, Fujimura Y, Miyata T. VWF73, a region from D1596 to R1668 of von Willebrand factor, provides a minimal substrate for ADAMTS-13. Blood 2004; 103:607–612.

38 Zhou W, Tsai HM. An enzyme immunoassay of ADAMTS13 distinguishes patients with thrombotic thrombocytopenic purpura from normal individuals and carriers of ADAMTS13 mutations. Thromb Haemost 2004; 91: 806–811.

39 Kokame K, Nobe Y, Kokubo Y, et al. FRETS-VWF73, a first fluorogenic substrate for ADAMTS13 assay. Br J Haematol 2005; 129:93–100.

40 • Wu JJ, Fujikawa K, Lian EC, et al. A rapid enzyme-linked assay for ADAMTS-13. J Thromb Haemost 2006; 4:129–136.
The authors developed a VWF73-based horseradish peroxidase-labeled substrate to assay for ADAMTS13 activity.

41 • Jin M, Cataland S, Bissell M, Wu HM. A rapid test for the diagnosis of thrombotic thrombocytopenic purpura using surface enhanced laser desorption/ionization time-of-flight (SELDI-TOF)-mass spectrometry. J Thromb Haemost 2006; 4: 333–338.
The authors developed an accurate and quantitative ADAMTS13 assay using mass spectrometry.

42 • Kato S, Matsumoto M, Matsuyama T, et al. Novel monoclonal antibody-based enzyme immunoassay for determining plasma levels of ADAMTS13 activity. Transfusion 2006; 46:1444–1452.
The authors developed a quantitative ADAMTS13 activity assay using a monoclonal antibody that specifically recognizes the cleavage of VWF73.

43 • Zhang L, Lawson HL, Harish VC, et al. Creation of a recombinant peptide substrate for fluorescence resonance energy transfer-based protease assays. Anal Biochem 2006; 358:298–300.
The authors developed a recombinant substrate for an ADAMTS13 assay based on fluorescence resonance energy transfer.

44 • Anderson PJ, Kokame K, Sadler JE. Zinc and calcium ions cooperatively modulate ADAMTS13 activity. J Biol Chem 2006; 281:850–857.
The enzyme-kinetic parameters of ADAMTS13 for the natural substrate VWF and the synthetic substrate FRETS-VWF73 are reported here.

45 Groot E, Hulstein JJ, Rison CN, et al. FRETS-VWF73: a rapid and predictive tool for thrombotic thrombocytopenic purpura. J Thromb Haemost 2006; 4:698–699.

46 Kremer Hovinga JA, Mottini M, Lammle B. Measurement of ADAMTS-13 activity in plasma by the FRETS-VWF73 assay: comparison with other assay methods. J Thromb Haemost 2006; 4:1146–1148.

47 Mahdian R, Rayes J, Girma JP, et al. Comparison of FRETS-VWF73 to full-length VWF as a substrate for ADAMTS13 activity measurement in human plasma samples. Thromb Haemost 2006; 95:1049–1051.

48 Nishio K, Anderson PJ, Zheng XL, Sadler JE. Binding of platelet glycoprotein Ibα to von Willebrand factor domain A1 stimulates the cleavage of the adjacent domain A2 by ADAMTS13. Proc Natl Acad Sci USA 2004; 101: 10578–10583.

49 Dong JF, Moake JL, Bernardo A, et al. ADAMTS-13 metalloprotease interacts with the endothelial cell-derived ultra-large von Willebrand factor. J Biol Chem 2003; 278:29633–29639.

50 Scheiflinger F, Knobl P, Trattner B, et al. Nonneutralizing IgM and IgG antibodies to von Willebrand factor-cleaving protease (ADAMTS-13) in a patient with thrombotic thrombocytopenic purpura. Blood 2003; 102: 3241–3243.

51 Rieger M, Mannucci PM, Kremer Hovinga JA, et al. ADAMTS13 autoantibodies in patients with thrombotic microangiopathies and other immunomediated diseases. Blood 2005; 106:1262–1267.

52 Tsai HM, Raoufi M, Zhou W, et al. ADAMTS13-binding IgG are present in patients with thrombotic thrombocytopenic purpura. Thromb Haemost 2006; 95:886–892.

53 Feys HB, Liu F, Dong N, et al. ADAMTS-13 plasma level determination
• uncovers antigen absence in acquired thrombotic thrombocytopenic purpura and ethnic differences. J Thromb Haemost 2006; 4:955–962.
This study reported that Chinese have significantly lower ADAMTS13 antigen levels.

54 Rieger M, Ferrari S, Kremer Hovinga JA, et al. Relation between ADAMTS13
• activity and ADAMTS13 antigen levels in healthy donors and patients with thrombotic microangiopathies (TMA). Thromb Haemost 2006; 95:212–220.
These workers established an ELISA assay for ADAMTS13 antigen levels and reported the median plasma ADAMTS13 level to be 1.08 mg/ml.

55 Soejima K, Nakamura H, Hirashima M, et al. Analysis on the molecular species
• and concentration of circulating ADAMTS13 in blood. J Biochem (Tokyo) 2006; 139:147–154.
In this study the plasma ADAMTS13 concentration was reported as 0.5–1 mg/ml and the extinction coefficient of recombinant ADAMTS13 was 1.7.

56 Banno F, Kaminaka K, Soejima K, et al. Identification of strain-specific variants of mouse Adamts13 gene encoding von Willebrand factor-cleaving protease. J Biol Chem 2004; 279:30896–30903.

57 Motto DG, Chauhan AK, Zhu G, et al. Shigatoxin triggers thrombotic thrombocytopenic purpura in genetically susceptible ADAMTS13-deficient mice. J Clin Invest 2005; 115:2752–2761.

58 Banno F, Kokame K, Okuda T, et al. Complete deficiency in ADAMTS13 is
•• prothrombotic, but it alone is not sufficient to cause thrombotic thrombocytopenic purpura. Blood 2006; 107:3161–3166.
The authors produced ADAMTS13-deficient mice that exhibited thrombocytopenia by the intravenous injection of collagen.

59 Chauhan AK, Motto DG, Lamb CB, et al. Systemic antithrombotic effects of
•• ADAMTS13. J Exp Med 2006; 203:767–776.
The authors demonstrated spontaneous thrombus formation in activated microvenules of Adamts13-deficient mice by intravital microscopy.

Age- and gender-related differences of plasma prothrombin activity levels

Toshiyuki Sakata[1], Akira Okamoto[1], Takashi Morita[2], Yoshihiro Kokubo[3], Kiyoshi Sato[1], Akira Okayama[3], Hitonobu Tomoike[3], Toshiyuki Miyata[4]

[1]Laboratory of Clinical Chemistry, National Cardiovascular Center, Suita, Osaka, Japan; [2]Department of Biochemistry, Meiji Pharmaceutical University, Kiyose, Tokyo, Japan; [3]Department of Preventive Cardiology and [4]Research Institute, National Cardiovascular Center, Suita, Osaka, Japan

Dear Sir,

Advancing age is an important risk factor for venous or arterial thrombosis in both sexes (1–3). Moreover, gender is associated with differences in the prothrombotic state and in the progression of atherosclerosis that occurs with aging (4, 5). Prothrombin is one of the dominant factors influencing thrombin generation (6), and the prothrombin G20210A mutation accompanied by an increased level of prothrombin poses a risk factor for venous or arterial thrombosis (7, 8). However, gender differences in age-related changes in plasma prothrombin activity have not been investigated until now. In the present study, we measured prothrombin activity in 742 individuals derived from a general Japanese population which was supposed to be free of prothrombin G20210A mutation (9).

The study population was composed of samples randomly selected from the residents of Suita, a city located in the second largest urban area in Japan (the Suita Study) (4). All subjects had been visiting the National Cardiovascular Center every two years since 1989 for regular health checkups. Only subjects who provided written informed consent to have a blood examination were enrolled in this study. We excluded subjects treated with oral anticoagulant therapy. Finally, 742 subjects, aged 36 to 85 years (mean age: 64 years), were included in this study. Spearman correlation analysis was used to assess the association between aging and the level of prothrombin activity within a given gender. For comparison between the two gender groups, the Mann-Whitney U test was used. Differences with a value of $p<0.01$ for the Spearman correlation analysis and $p<0.05$ for the Mann-Whitney U test were considered to be significant. Statistical calculations were performed using SPSS version 12.0 (SPSS Inc, Chicago, IL, USA). Prothrombin activity was measured according to a published method (10) with a modification. Briefly, 200 µl of 20 mM Tris-HCl, 0.14 M NaCl, pH 7.5 buffer containing 1 mg/ml of bovine serum albumin (TBSA) was added to 50 µl of plasma anticoagulated with 0.13% sodium citrate. Then, diluted plasma was incubated for 150 seconds at 37°C, and we detected ΔA/min at 405 nm after adding 50 µl of the reagent containing 6 mM $CaCl_2$, 0.5 mM Boc-Val-Pro-Arg-pNA as a thrombin substrate, 500 pM carinactivase-1 as a thrombin activator, and TBSA. Calibration was performed with a standard-human-plasma (Dade Behring GmbH, Marburg, Germany). The coefficient of intra-assay variation for prothrombin activity assay was 2.0%.

The mean ± SD of prothrombin activity level in men and women was 110.2 ± 17.0 (range: 54.5–158.5%) and 120.4 ± 17.4 (range: 57.5–194.4%), respectively. Figure 1 shows the age-related distribution (36–85 years) of prothrombin activity in 348 men (Fig. 1A) and 394 women (Fig. 1B). As a whole, a linear decrease of prothrombin activity level with age was observed in

Correspondence to:
Toshiyuki Sakata, PhD
Laboratory of Clinical Chemistry, National Cardiovascular Center
Fujishirodai 5–7–1, Suita, Osaka 565–8565, Japan
Tel.: +81 6 6833 5012 ext. 2296, Fax: +81 6 6835 1176
E-mail: tsakata@hsp.ncvc.go.jp

Received January 10, 2007
Accepted after revision March 20, 2007

Prepublished online May 3, 2007
doi:10.1160/TH07-01-0019

Thromb Haemost 2007; 97: 1052–1053

men (r=-0.34, p<0.0001), but not in women (r=-0.04, p=0.47). When prothrombin activity level was analyzed in 10-year age groups, significant decreases were observed in the men aged 46–55 years and 56–65 years (p<0.0001), aged 56–65 years and 76–85 years (p<0.05), and in the women aged 66–75 years and 76–85 years (p<0.0001). Levels of prothrombin activity were decreased in both sexes in the oldest age group (aged 76–85 years). With regards to gender-related change, the prothrombin activity level in the age group of 56–65 years, 66–75 years, and 76–85 years was significantly lower in men than in women.

In the present study, we showed the age-related decrease in the plasma prothrombin activity of men and gender-related change in the plasma prothrombin activity. These results contribute to the understanding of age-related hypercoagulability and to the practical institution of anticoagulant therapy in older patients. It has been established that thrombin generation increases with age in both sexes, evidenced by plasma prothrombin fragment F1+2 levels produced by the cleavage of prothrombin by factor Xa (11, 12). Age-related hypercoagulability does not likely stem from the prothrombin activity, because the prothrombin activity of men showed the age-related decrease, but it may result from some other mechanisms including decreased levels of anticoagulant proteins such as protein C and S (11, 13). We presented here the gender-related change of significantly lower prothrombin activity levels in men in the age of 56–85 years than in women. Men tend to develop thrombotic events including recurrent venous thrombosis (14), but this tendency was not related to the plasma level of prothrombin activity. Our work sheds further light on the point that, when considering relative hypercoagulability, gender-adjustment is necessary for the comparison of prothrombin activity levels.

With regards to anticoagulant therapy, the plasma levels of vitamin K-dependent coagulation factors decrease with increasing intensity of anticoagulation therapy (15). At the same time, the risks of major haemorrhage increase according to the intensity of anticoagulation therapy, especially in patients older than 80 years (16). Given our current study results, the markedly decreased prothrombin level in the age group of 76–85 years, especially in men, provides a potential mechanistic explanation for the increased rate of major haemorrhage observed in elderly patients receiving anticoagulant therapy.

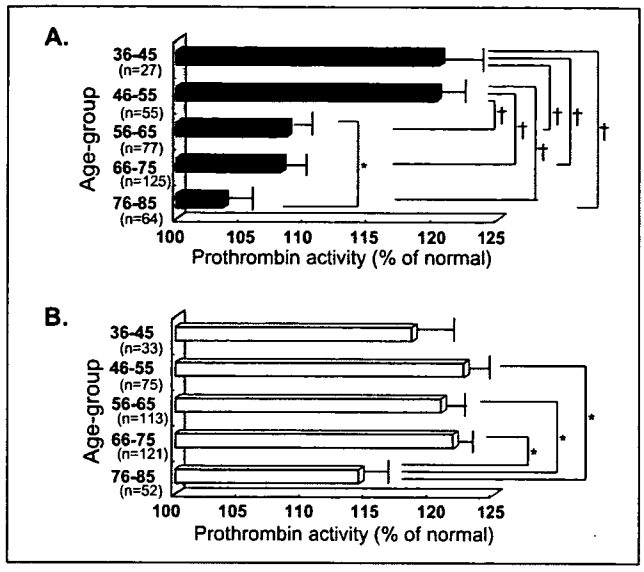

Figure 1: Age-related changes of plasma prothrombin activity levels according to gender (A: men, B: women). Populations aged from 36 to 85 years old were divided into five age groups by gender. Data are expressed as the mean ± SEM. *: P<0.05, †: P<0.0001, compared between two age groups of the same gender.

In conclusion, there are significant age- and gender-related differences in plasma prothrombin activity levels. In particular, the prothrombin activity level in men in the age group of 76–85 years was lower than that of any other age group in either gender.

Acknowledgments

This study was supported by the Program for Promotion of Fundamental Studies in Health Sciences of the National Institute of Biomedical Innovation (NIBIO), a Grant-in-Aid from the Ministry of Health, Labor, and Welfare of Japan, and the Ministry of Education, Culture, Sports, Science, and Technology of Japan.

References

1. White RH. The epidemiology of venous thromboembolism. Circulation 2003; 107: I4–8.
2. Feinbloom D, Bauer KA. Assessment of hemostatic risk factors in predicting arterial thrombotic events. Arterioscler Thromb Vasc Biol 2005; 25: 2043–2053.
3. Couturaud F, Kearon C, Leroyer C, et al. Incidence of venous thromboembolism in first-degree relatives of patients with venous thromboembolism who have factor V Leiden. Thromb Haemost 2006; 96: 744–749.
4. Mannami T, Baba S, Ogata J. Strong and significant relationships between aggregation of major coronary risk factors and the acceleration of carotid atherosclerosis in the general population of a Japanese city: the Suita Study. Arch Intern Med 2000; 160: 2297–2303.
5. Tofler GH, Massaro J, Levy D, et al. Relation of the prothrombotic state to increasing age (from the Framingham Offspring Study). Am J Cardiol 2005; 96: 1280–1283.
6. Butenas S, van't Veer C, Mann KG. "Normal" thrombin generation. Blood 1999; 94: 2169–2178.
7. Poort SR, Rosendaal FR, Reitsma PH, et al. A common genetic variation in the 3'-untranslated region of the prothrombin gene is associated with elevated plasma prothrombin levels and an increase in venous thrombosis. Blood 1996; 88: 3698–3703.
8. Ye Z, Liu EH, Higgins JP, et al. Seven haemostatic gene polymorphisms in coronary disease: meta-analysis of 66,155 cases and 91,307 controls. Lancet 2006; 367: 651–658.
9. Miyata T, Kawasaki T, Fujimura H, et al. The prothrombin gene G20210A mutation is not found among Japanese patients with deep vein thrombosis and healthy individuals. Blood Coagul Fibrinolysis 1998; 9: 451–452.
10. Yamada D, Morita T. CA-1 method, a novel assay for quantification of normal prothrombin using a Ca2+-dependent prothrombin activator, carinactivase-1. Thromb Res 1999; 94: 221–226.
11. Bauer KA, Weiss LM, Sparrow D, et al. Aging-associated changes in induces of thrombin generation and protein C activation in humans. J Clin Invest 1987; 80; 1527–1534.
12. Mari D, Mannucci PM, Coppola R, et al. Hypercoagulability in centenarians: the paradox of successful aging. Blood 1995; 85: 3144–3149.
13. Miyata T, Kimura R, Kokubo Y, et al. Genetic risk factors for deep vein thrombosis among Japanese: Importance of protein S K196E mutation. Int J Hematol 2006; 83; 217–223.
14. White RH, Dager WE, Zhou H, et al. Racial and gender differences in the incidence of recurrent venous thromboembolism. Thromb Haemost 2006; 96: 267–273.
15. Sakata T, Kario K, Matsuo T, et al. Suppression of plasma activated factor VII levels by warfarin therapy. Arterioscler Thromb Vasc Biol 1995; 15; 241–246.
16. White RH, McBurnie MA, Manolio T, et al. Oral anticoagulation in patients with atrial fibrillation: adherence with guidelines in an elderly cohort. Am J Med 1999; 106; 165–171.

Impaired Mast Cell Maturation and Degranulation and Attenuated Allergic Responses in Ndrg1-Deficient Mice[1]

Yoshitaka Taketomi,*† Kohei Sunaga,† Satoshi Tanaka,[2¶] Masanori Nakamura,‡ Satoru Arata,* Tomohiko Okuda,[3#] Tae-Chul Moon,* Hyeun-Wook Chang,* Yukihiko Sugimoto,[¶] Koichi Kokame,# Toshiyuki Miyata,# Makoto Murakami,[†§**] and Ichiro Kudo[4†]

We have previously reported that N-myc downstream regulated gene-1 (NDRG1) is an early inducible protein during the maturation of mouse bone marrow-derived mast cells (BMMCs) toward a connective tissue mast cell-like phenotype. To clarify the function of NDRG1 in mast cells and allergic responses, we herein analyzed mast cell-associated phenotypes of mice lacking the Ndrg1 gene. Allergic responses including IgE-mediated passive systemic and cutaneous anaphylactic reactions were markedly attenuated in Ndrg1-deficient mice as compared with those in wild-type mice. In Ndrg1-deficient mice, dermal and peritoneal mast cells were decreased in number and morphologically abnormal with impaired degranulating ability. Ex vivo, Ndrg1-deficient BMMCs cocultured with Swiss 3T3 fibroblasts in the presence of stem cell factor, a condition that facilitates the maturation of BMMCs toward a CTMC-like phenotype, displayed less exocytosis than replicate wild-type cells after the cross-linking of Fc•RI or stimulation with compound 48/80, even though the exocytotic response of IL-3-maintained, immature BMMCs from both genotypes was comparable. Unlike degranulation, the production of leukotriene and cytokines by cocultured BMMCs was unaffected by NDRG1 deficiency. Taken together, the altered phenotypes of Ndrg1-deficient mast cells both in vivo and ex vivo suggest that NDRG1 has roles in the terminal maturation and effector function (degranulation) of mast cells. The Journal of Immunology, 2007, 178: 7042–7053.

Mast cells have long been considered to serve primarily as important effector cells for acute IgE-associated allergic reactions such as anaphylaxis, rhinitis, and asthma. Mast cells are tissue-resident cells of hemopoietic origin, representing an important source of a variety of inflammatory mediators such as vasoactive amines, proteases, eicosanoids, cytokines, and chemokines. They orchestrate various aspects of the IgE-associated and even IgE-independent immune responses not only through the release of these mediators but also through cell-cell interaction by which they regulate the function of other cells.

It has been elucidated that mast cells originate from hemopoietic stem cells in vivo (1) or multipotential progenitors in vitro (2). Mast cell precursors circulate in the blood and migrate into connective or mucous tissues where they differentiate into mature mast cell phenotypes depending on the microenvironment of the tissue (3–6). Stem cell factor (SCF)[5] and its receptor c-kit are prerequisites for the homing and subsequent differentiation of mast cells in the whole tissue (7, 8), and the $\bullet_4\bullet_7$ integrin (9) and the chemokine receptor CXCR2 (10) have additional and profound influences on the basal homing, establishment, and maintenance of mast cells in the small intestine. However, the precise mechanism underlying the tissue-based maturation of mast cells is still a challenging area in this field of research.

Coculture of IL-3-maintained immature mouse bone marrow-derived mast cells (BMMCs), a progenitor population of mast cells, with fibroblasts is a useful system for analyzing certain aspects of change into a connective tissue mast cell (CTMC)-like phenotype (11–14). We have developed a unique mast cell maturation system by which BMMCs cocultured with Swiss 3T3 fibroblasts in the presence of soluble SCF alter their morphological and functional properties from an immature to a mature CTMC-like phenotype after only 4–6 days of coculture (14). Following cDNA subtraction between BMMCs before and after such coculture, we have identified N-myc downstream regulated gene-1 (NDRG1) as the most frequently induced gene during the maturation of BMMCs into a mature CTMC-like phenotype under these conditions (15, 16). Moreover, the overexpression of NDRG1 in the rat mastocytoma RBL-2H3 augments exocytotic degranulation in response to IgE-dependent and

*Center for Biotechnology, †Department of Health Chemistry, School of Pharmaceutical Sciences, and ‡Department of Oral Anatomy and Developmental Biology, School of Dentistry, Showa University, Tokyo, Japan; §Tokyo Metropolitan Institute of Medical Science, Tokyo, Japan; ¶Department of Physiological Chemistry, Faculty of Pharmaceutical Sciences, Kyoto University, Kyoto, Japan; *College of Pharmacy, Yeungnam University, Gyonsan, Korea; #National Cardiovascular Center Research Institute, Osaka, Japan; and **Precursory Research for Embryonic Science and Technology, Japan Science and Technology Agency, Saitama, Japan

Received for publication August 9, 2006. Accepted for publication February 27, 2007.

The costs of publication of this article were defrayed in part by the payment of page charges. This article must therefore be hereby marked advertisement in accordance with 18 U.S.C. Section 1734 solely to indicate this fact.

[1] This work was supported by a Showa University special grant-in-aid for innovative collaborative research projects and a special research grant-in-aid for development of characteristic education from the Ministry of Education, Culture, Sports, Science, and Technology of Japan. M.M. was supported by Precursory Research for Embryonic Science and Technology, Japan Science and Technology Agency.

[2] Current address: Department of Immunobiology, School of Pharmaceutical Sciences, Mukogawa Women's University, Hyogo, Japan.

[3] Current address: COE Formation for Genomic Analysis of Disease Model Animals with Multiple Genetic Alterations, Graduate School of Medicine, Kyoto University, Kyoto, Japan.

[4] Address correspondence and reprint requests to Dr. Ichiro Kudo, Department of Health Chemistry, School of Pharmaceutical Sciences, Showa University, 1-5-8 Hatanodai, Shinagawa-ku, Tokyo, Japan. E-mail address: ichi-ku@pharm.showa-u.ac.jp

[5] Abbreviations used in this paper: SCF, stem cell factor; NDRG1, N-myc downstream regulated gene-1; BMMC, bone marrow-derived mast cell; CMT4D, Charcot-Marie-Tooth disease type 4D; CPA, carboxypeptidase A; CTMC, connective tissue mast cell; HSA, human serum albumin; •-HEX, •-hexosaminidase; LT, leukotriene; lyso-PS, lysophosphatidyl-$_L$-serine; mMCP, mouse mast cell protease; PCA, passive cutaneous anaphylaxis; PLC, phospholipase C; PMC, peritoneal mast cell.

-independent stimuli (15), suggesting that NDRG1 is involved in the divergent signaling pathways leading to exocytosis at their point of convergence or beyond or that it allows immature mast cells to differentiate into a mature phenotype that degranulates more efficiently in response to various secretagogues.

NDRG1, an intracellular protein with an • • hydrolase fold (17) and three unique tandem repeats of 10 hydrophilic amino acids near the COOH-terminal end is a member of the emerging NDRG family that also contains NDRG2, NDRG3, and NDRG4 (18–20). NDRG1 has been independently identified as a molecule whose expression is markedly altered in several cell types under various conditions such as cellular stress response, hypoxia, and cell differentiation (15, 21–27). Significantly, the forcible expression of NDRG1 in cancer cells decreases their growth rate and metastasis by inducing cell differentiation and reversing their propensity to metastasize (28, 29), suggesting that NDRG1 is a cell differentiation regulator. Recently, a nonsense mutation in the Ndrg1 gene has been reported to be responsible for hereditary motor and sensory neuropathy-Lom, a severe autosomal recessive peripheral neuropathy known as Charcot-Marie-Tooth disease type 4D (CMT4D) (30, 31). Furthermore, mice lacking the Ndrg1 gene exhibit a peripheral neuropathy characterized by demyelination, a symptom similar to that observed in patients with CMT4D (32). These observations suggest that NDRG1 is essential for axon survival and appropriate differentiation, although the molecular machinery responsible for the neuronal function of NDRG1 still awaits further study.

To gain further insights into the functional role of this unique protein in mast cells, we have herein analyzed the mast cell-related phenotypes of Ndrg1-deficient mice. We found that the Ndrg1-deficient mice had mitigated passive systemic and local anaphylactic responses and that the mast cells from these mice were morphologically and functionally abnormal in terms of their aberrant granule structure and reduced exocytotic capacity. Thus, our findings provide unequivocal evidence that NDRG1 is a critical modulator of the maturation, and thereby the function, of mast cells.

Materials and Methods

Mice

The construction of the Ndrg1-deficient mice was described previously in detail (32). These Ndrg1-deficient mice were further backcrossed 10 generations onto a C57BL/6 background. All mice were bred in our animal facility under specific pathogen-free conditions. Mast cell-deficient $WBB6F_1$-W/W^v (W/W^v) and littermate control $WBB6F_1$-• /• mice were purchased from Japan SLC. We used 8- to 12-wk-old mice for all experiments. The genotypes of Ndrg1$^{•/•}$ and Ndrg1$^{•/•}$ were confirmed by PCR analysis of tail biopsies as described (32).

Passive systemic anaphylaxis

The anaphylaxis method used was described previously (33). Briefly, mice were administered 3 • g of anti-DNP mouse monoclonal IgE (SPE-7; Sigma-Aldrich) in 200 • l of saline i.v. through the tail vein. Then, 24 h later, the mice were challenged i.v. with 500 • g of DNP-conjugated human serum albumin (HSA) (DNP-HSA; Sigma-Aldrich) in 200 • l of saline. After Ag challenge, body temperature was monitored at various intervals using a rectal probe coupled to a digital thermometer (BAT-12R and RET-3; Physitemp Instruments). Blood samples were collected by puncturing the hearts of the sacrificed mice 1.5 min after Ag challenge. The sera were prepared and treated with 3% perchloric acid for the removal of proteins. The resulting supernatants were subjected to measurement of histamine. Histamine was separated by HPLC on a cation-exchange WCX-1 column (Shimadzu) and then measured fluorometrically by the o-phthalaldehyde method (34).

Passive cutaneous anaphylaxis (PCA)

The left and right ears of the mice were treated intradermally with 25 ng of anti-DNP IgE in 25 • l of saline. Then, 24 h later the mice were challenged i.v. through the tail vein with various doses of DNP-HSA together with 1 mg of Evans blue (Wako Pure Chemical) in 200 • l of saline. At various intervals after the Ag challenge, extravasation was visualized by blue staining of the ear skin. The ears were removed and incubated at 37°C in 1 ml of 3 N KOH. On the following day the mixtures were extracted with 1.24 M phosphoric acid and acetone. Absorbance of the resulting supernatants was measured at 620 nm. The relationship between Evans blue concentration and absorbance was linear, indicating that the absorbance represented the quantity of Evans blue extravasation. Ear thickness was recorded 30 min after Ag challenge using a dial thickness gauge (Mitutoyo Corporation) with a minimum sensitivity of 1 • m. Changes in ear thickness were determined as the difference before and after Ag challenge. For IgE-independent, compound 48/80-induced anaphylaxis, the ears were treated intradermally with various doses of compound 48/80 (Sigma-Aldrich) in 25 • l of saline followed by i.v. injection of 1 mg of Evans blue in 200 • l of saline. After 30 min, Evans blue extravasation was measured in a similar way.

Histological analysis

In a series of IgE-mediated, Ag-dependent PCA experiments, Ndrg1$^{•/•}$ and Ndrg1$^{•/•}$ mice were sacrificed before and after Ag challenge. The left and right ears were removed, fixed in 4% paraformaldehyde, and embedded in paraffin. Sections (5-• m thick) were cut and then stained with 0.05% acidic toluidine blue (pH 1.0). Intact and degranulated tissue mast cells were counted in the skin sections under an optical microscope (Axioskop 2 FS plus; Carl Zeiss MicroImaging) at • 100 magnification. Degranulated tissue mast cells were defined as those showing the release of • 10% cellular granules.

For transmission electron microscopy, ears were fixed with 2.5% glutaraldehyde in 0.1 M sodium cacodylate buffer (pH 7.2), postfixed with 2% OsO_4, dehydrated by a graded ethanol series, passed through propylene oxide, and then embedded in Epon 812. Ultrathin sections (0.08-• m thick) were stained with uranyl acetate and lead citrate and then examined using an electron microscope (H-7600; Hitachi).

For immunohistochemistry, cytospin preparations were incubated with 5% normal rabbit serum in PBS containing 5% BSA and 0.025% Triton X-100 for 1 h and then with goat anti-NDRG1 polyclonal Ab (N-19; Santa Cruz Biotechnology) at 1/100 dilution in the same buffer at 4°C overnight. These preparations were incubated with biotinylated rabbit anti-goat IgG (Vector Laboratories) at 1/100 dilution in PBS containing 5% BSA, 0.025% Triton X-100, and 10% mouse serum for 30 min followed by incubation with avidin DH and biotinylated HRP (Vectastain ABC kit; Vector Laboratories). After 30 min these preparations were stained with 0.5 mg/ml 3,3•-diaminobenzidine and 0.1% hydrogen peroxide solution.

Preparation and activation of peritoneal mast cells (PMCs)

To harvest peritoneal cells, 5 ml of HBSS was injected into the mouse peritoneal cavity and the abdomen was massaged gently. After the fluid containing peritoneal cells had been collected and centrifuged, the pellets were resuspended in PIPES-buffered saline. The cells were cytospun onto glass slides for 5 min and then incubated for 30 min with 1% Alcian blue (pH 2.5) and counterstained for 3 min with 0.1% safranin O.

For degranulation analysis, 10^6 peritoneal cells were incubated for 1 h in culture medium containing 100 ng/ml SCF and 10 • g/ml anti-DNP IgE and then treated for 30 min with 100 ng/ml DNP-BSA as an Ag and 4 • M 1-oleoyl-2-hydroxy-sn-glycero-3-phosphoryl-$_L$-serine (lyso-PS; Avanti Polar Lipids) as a cofactor in the same buffer. The contents of • -hexosaminidase (• -HEX) in both supernatants and cell pellets were then measured by triplicate. The percentage releases were calculated using the formula [S/(S • P)] • 100, where S and P are the • -HEX contents of the supernatants and cell pellets, respectively, from each sample. • -HEX assay was performed as described previously (35).

Analyses of protease activities

The chromogenic peptide substrates S-2586 (3-carbomethoxypropionyl-$_L$-arginyl-$_L$-propyl-$_L$-tyrosine-p-nitroaniline) and S-2288 (H-$_D$-isoleucyl-$_L$-propyl-arginine-p-nitroaniline) were purchased from Chromogenix, and M-2245 (N-(4-methoxyphenylazoformyl)-Phe-OH) from Bachem.

Ear extracts were obtained by the addition of 1 ml of PBS containing 2 M NaCl per ear, followed by homogenization using a PT3100 Polytron device (Kinematica). After homogenization, Triton X-100 was added to give a final concentration of 0.5%. The extracts were centrifuged at 10,000 • g, and 10-• l aliquots of the resultant supernatants were diluted with 90 • l of H_2O followed by incubation with 20 • l of 1.8 mM solution (in H_2O) of the chromogenic substrates S-2586 (for chymotrypsin-like proteases), S-2288 (for trypsin-like proteases), and M-2245 (for carboxypeptidase A (CPA)) at 37°C. Changes in absorbance at 405 nm were measured as described previously (36).

Culture of primary and maturated BMMCs

Bone marrow cells were obtained from the femurs and tibias of mice and cultured in IL-3-containing BMMC-complete medium comprising DMEM, 10% FBS, 2 mM L-glutamine, 100 IU/ml penicillin, 100 • g/ml streptomycin, 100 mM nonessential amino acids, and 5 ng/ml mouse rIL-3. Nonadherent cells were transferred to fresh IL-3-containing BMMC-complete medium at least once a week. After 4–5 wk of culture, the majority of the floating cells were confirmed to be immature mast cells as assessed by Alcian blue-positive and safranin-negative staining of their granules.

The maturation of immature BMMCs toward CTMC-like cells was described previously in detail (14). Briefly, 5 • 10^6 BMMCs were seeded on the subconfluent Swiss 3T3 fibroblast monolayer in 100-mm culture dishes and cocultured for 4–6 days in the presence of 50 ng/ml SCF with replacement of the medium every 2 days. The cells were trypsinized and replated, and nonadherent cells (• 95% were mast cells) were collected and used for analyses. The maturation of BMMCs into CTMC-like cells was verified by staining of their granules with Alcian blue and counterstaining with safranin O.

Western blotting

BMMCs (10^5) were lysed in SDS-PAGE sample buffer (63 mM Tris-HCl (pH 6.8), 2% SDS, 10% glycerol, and 0.08% bromophenol blue) containing 5% 2-ME and subjected to SDS-PAGE. Proteins were subsequently blotted onto nitrocellulose membranes, followed by blocking with 5% milk powder in PBS containing 0.05% Tween 20. The membranes were incubated for 1 h with rabbit anti-mouse NDRG1 polyclonal Ab (15) followed by reprobing with mouse anti-• -tubulin mAb (Zymed Laboratories) at 1/5000 dilution in PBS with 0.05% Tween 20. Tyrosine phosphorylation of phospholipase C (PLC) •1 and •2 was determined by immunoblotting with rabbit anti-human phospho-PLC•1 (Tyr^{783}) and •2 (Tyr^{1217}) polyclonal Abs followed by reprobing with rabbit anti-human PLC•1 and •2 polyclonal Abs (Cell Signaling Technology) at 1/1000 dilution in PBS with 0.05% Tween 20 (37). After washing with PBS and 0.05% Tween 20, the membranes were incubated with a secondary anti-rabbit Ig Ab conjugated with HRP (Zymed) at 1/5000 dilution in PBS plus 0.05% Tween 20. After 1 h of incubation the membranes were washed extensively with PBS plus 0.05% Tween 20 followed by washing with PBS without detergent. The membranes were developed with the ECL system (PerkinElmer Life Sciences) according to the protocol provided by the manufacturer.

RT-PCR

Total RNA was extracted from BMMCs with TRIzol reagent (Invitrogen Life Technologies). First-strand cDNA synthesis was conducted using the SuperScript III reverse transcriptase kit (Invitrogen Life Technologies). Five micrograms of total RNA was used in reactions primed with oligo(dT) (12–18-mer) primer (Invitrogen Life Technologies) to obtain cDNA. Then, 1 •l of the synthesized cDNA was used as the template for the mRNA amplification reactions. The PCR amplification was performed using a GeneAmp PCR System 9600 (PerkinElmer) using a standard PCR protocol. The RT-PCR product was analyzed on a 1.5% agarose gel and visualized using ethidium bromide staining.

The primer pairs for NDRG1, NDRG2, NDRG3, and NDRG4 were described previously (32). The primer pairs were 5•-ACCACATTCTCGC CCTTACAT-3• and 5•-TCTCAGTTTCACCTCCCTCAG-3• for mouse mast cell protease (mMCP)-4; 5•-ATAACAGTCCTCCTAGGAGCC-3• and 5•-GATCCAGGGCCTGTAATGGGA-3• for mMCP-5; 5•-GCACA TCAAAAGCCCACAGC-3• and 5•-TAGACAGGGGAGACAGAGGA C-3• for mMCP-6; 5•-CAGGCAGGCACAGTTATGCAA-3• and 5•-A ACCCAGTCTAAGGAAGACC-3• for mMC-CPA3; 5•-ATGGAGACC CCATTGCTCTGA-3• and 5•-ATGATCTCCATTGAGGCTGCC-3• for N-deacetylase/N-sulfotransferase-2; 5•-CAGCTAGTTGTCAATCCTGCTCT TC-3• and 5•-GGTGCAGCTTATCGATGAATCCAG-3• for IL-4; 5•-CAG AGGATACCACTCCCAACAGAC-3• and 5•-CCTTAGCCACTCCTTCTG TGACTC-3• for IL-6; 5•-GAAAGCATGATCCGCGACGTGGAA-3• and 5•-GCTGACGGTGTGGGTGAGGAGCAC-3• for TNF-•; and 5•-TCGTGGA TCTGACGTGCCGCCTG-3• and 5•-CACCACCCTGTTGCTGTAGCCGT AT-3• for GAPDH.

Flow cytometry

Suspensions of 10^6 BMMCs were treated with rat anti-mouse CD16/CD32 (Fc•RII/RIII) mAb (clone 2.4G2, BD Biosciences Pharmingen) (final concentration, 10 • g/ml) in 2% FBS-PBS for 10 min on ice to block cell surface Fc•Rs, followed by incubation for 45 min with FITC-labeled rat anti-mouse CD117 (c-kit) mAb (clone 2B8, BD Biosciences) at 1/50 dilution in the same buffer. To assess Fc•RI expression, the cells were treated for 3 h with 10 • g/ml mouse IgE (SPE-7). Fc•Rs were blocked as described above and the cells were subsequently incubated with PE-labeled rat anti-mouse IgE mAb (clone 23G3; eBioscience) at 1/50 dilution in 2% FBS-PBS. Flow cytometry was conducted on a FACSCalibur instrument (BD Biosciences).

Activation of BMMCs

For stimulation with IgE plus polyvalent Ag (DNP-BSA), BMMCs (10^7 cells/ml) before and after coculture with fibroblasts were sensitized with 100 ng/ml anti-DNP IgE for 1 h at 37°C. After washing with medium, the cells were stimulated for appropriate periods with various doses of DNP-BSA at 37°C. For stimulation with compound 48/80, the cells were treated for the appropriate periods with various doses of compound 48/80 at 37°C. The resulting supernatants and cell pellets were then taken for a • -HEX assay. The cysteinyl leukotriene (LT) C_4 (LTC_4) production was determined using enzyme immunoassay kits according to the manufacturer's instructions (Cayman Chemical). Replicate cells were subjected to RNA extraction followed by RT-PCR for several cytokines, as noted above.

Statistical analysis

Results from in vivo and ex vivo experiments (mean • SEM) were assessed with Student's unpaired, two-tailed t test. Differences between replicate $Ndrg1^{\bullet/\bullet}$ and $Ndrg1^{\bullet/\bullet}$ groups were regarded as significant at p • 0.05, unless otherwise stated.

Results

Impaired mast cell-associated anaphylactic reactions in Ndrg1-deficient mice

Anaphylaxis represents an extreme form of mast cell-associated allergic reaction consisting of a sensitization phase in which allergen-specific IgE is produced and binds to mast cell surfaces and a subsequent acute effector phase in which allergen-induced activation of mast cells leads to the release of copious amounts of vasoactive amines and other inflammatory mediators (38). To clarify the in vivo role of NDRG1 in mast cell biology, we first examined the mast cell-dependent, IgE-mediated passive systemic anaphylactic reaction in Ndrg1-deficient mice.

$Ndrg1^{\bullet/\bullet}$ and $Ndrg1^{\bullet/\bullet}$ mice were sensitized with IgE directed against DNP and challenged 24 h later with DNP-HSA as an Ag, and their rectal temperatures were monitored at regular intervals. As shown in Fig. 1A, a temporary decrease in rectal temperature was observed in $Ndrg1^{\bullet/\bullet}$ mice 10–20 min after antigenic challenge, whereas such a decrease was virtually absent from mast cell-deficient W/W^v mice. Notably, although a significant decrease in rectal temperature following antigenic challenge was observed in $Ndrg1^{\bullet/\bullet}$ mice, it was modest in comparison with that in $Ndrg1^{\bullet/\bullet}$ mice. Serum samples were taken from these mice 1.5 min after Ag challenge for the determination of histamine concentration. As shown in Fig. 1B, $Ndrg1^{\bullet/\bullet}$ mice showed a marked increase in the serum histamine level upon the cross-linking of Fc•RI, whereas no appreciable increase was evident in W/W^v mice. Although there was a significant increase of the serum histamine level in Ag-challenged $Ndrg1^{\bullet/\bullet}$ mice compared with that in W/W^v mice, it reached a mean value of only 37% relative to that in replicate $Ndrg1^{\bullet/\bullet}$ mice (21.1 • 1.6 vs 7.9 • 1.6 nM in $Ndrg1^{\bullet/\bullet}$ and $Ndrg1^{\bullet/\bullet}$ mice, respectively; p • 0.01, n • 11).

To further assess the role of NDRG1 in anaphylaxis, we next investigated the capacity of Ndrg1-deficient mice to respond to immune challenge in PCA, where local extravasation and tissue swelling are induced by the local application of Ag-specific IgE followed by i.v. challenge of Ag. The ears of $Ndrg1^{\bullet/\bullet}$ and $Ndrg^{\bullet/\bullet}$ mice were injected intradermally with DNP-specific IgE and challenged 24 h later with an i.v. injection of DNP-HSA together with Evans blue dye. Mediators released upon mast cell activation increase vascular permeability, which allows the dye to leak from blood vessels into the surrounding tissue, causing edema and providing a measure of mast cell activation.

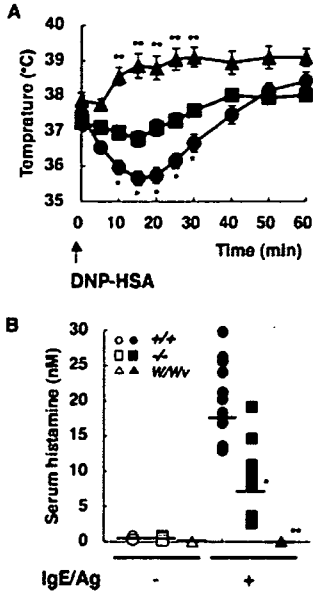

FIGURE 1. Effects of NDRG1 deficiency on IgE-mediated, Ag-dependent passive systemic anaphylaxis as assessed by rectal temperature change and serum histamine concentration. A, Ndrg1$^{-/-}$ (circles; n • 13), Ndrg1$^{+/+}$ (squares; n • 13), and WBB6F$_1$-W/W^v (W/W^v, triangles; n • 3) mice were sensitized with anti-DNP IgE and challenged with DNP-HSA to induce systemic anaphylaxis as described in Materials and Methods. Passive systemic anaphylactic response was monitored by measuring rectal temperatures at the indicated times after antigenic challenge. B, The histamine concentrations in sera from individual Ndrg1$^{-/-}$ (• /• , n • 11), Ndrg1$^{+/+}$ (• /• , n • 11), and WBB6F$_1$-W/W^v (W/W^v, n • 3) mice after Ag challenge for 30 min (filled symbols) or no stimulation (open symbols) were plotted, with the mean value for each group indicated by a line. •, p • 0.01 vs Ndrg1$^{-/-}$; and ••, p • 0.01 vs Ndrg1$^{-/-}$ mice.

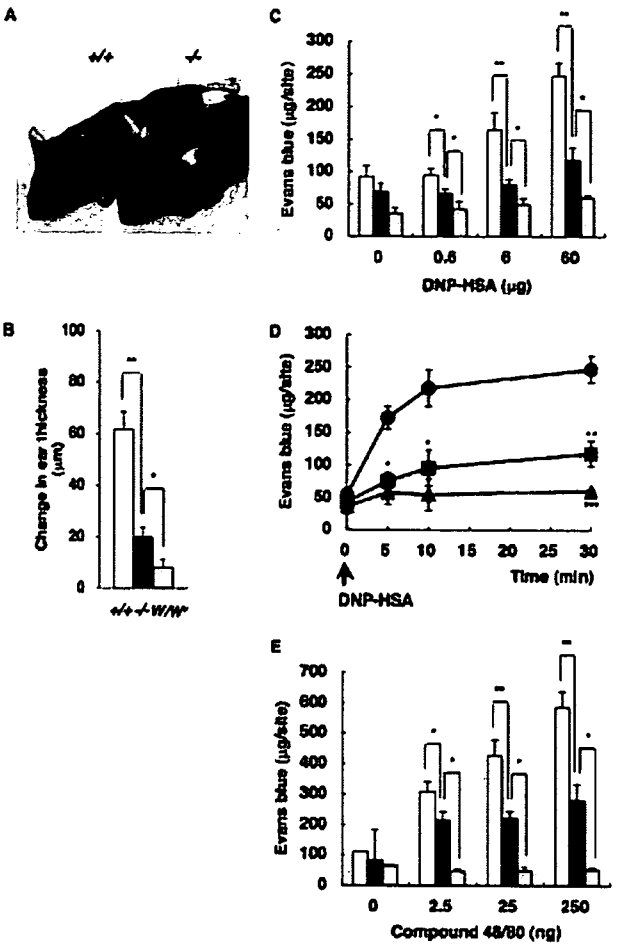

FIGURE 2. Effects of NDRG1 deficiency on PCA as assessed by ear swelling and Evans blue extravasation. Ndrg1$^{-/-}$ (• /•), Ndrg1$^{+/+}$ (• /•), and WBB6F$_1$-W/W^v (W/W^v) mice were sensitized with anti-DNP IgE and challenged 24 h later with DNP-HSA (A–D) or directly treated with compound 48/80 (E) together with Evans blue to induce PCA as described in Materials and Methods. A, Dye extravasation following administration of 60 • g of Ag was visualized by blue staining at the injection sites in the ears of Ndrg1$^{+/+}$ and Ndrg1$^{-/-}$ mice. Photographs of the mice were taken 30 min after Ag challenge. One representative of 11 mice for each genotype is shown. B, Ear thickness of Ndrg1$^{-/-}$ (n • 15), Ndrg1$^{+/+}$ (n • 15), and W/W^v (n • 6) mice was measured before and 30 min after Ag challenge using a dial thickness gauge. Ear thickness change, which represents the degree of ear swelling, was determined as the difference before and after Ag challenge into the right and left ears of each mouse. ••, p • 0.01; and •, p • 0.05. C, Dose-dependent extravasation of Evans blue into the ears of mice following IgE-mediated, Ag-dependent PCA. Ears of the IgE-sensitized Ndrg1$^{+/+}$ (open bars), Ndrg1$^{-/-}$ (filled bars), and W/W^v (gray bars) mice were challenged with 0 (n • 3), 0.6 (n • 9), 6 (n • 10), and 60 (n • 18) • g of DNP-HSA for 30 min. Extravasation of Evans blue was quantified as described in Materials and Methods. ••, p • 0.01 and •, p • 0.05. D, Kinetics of extravasation of Evans blue into the ears of mice following IgE-mediated, Ag-dependent PCA. Ears of the IgE-sensitized Ndrg1$^{+/+}$ (circles, n • 18, respectively), Ndrg1$^{-/-}$ (squares; n • 13, respectively), and W/W^v (triangles; n • 4, respectively) mice were challenged with 60 • g of DNP-HSA for the indicated periods. •, p • 0.01; and ••, p • 0.05 vs Ndrg1$^{-/-}$ mice. •••, p • 0.05 vs Ndrg1$^{-/-}$ mice. E, Dose-dependent extravasation of Evans blue into the ears of mice following compound 48/80-induced PCA. The left and right ears of Ndrg1$^{+/+}$ (open bars), Ndrg1$^{-/-}$ (filled bars), and W/W^v (gray bars) mice were treated with 0 (n • 3), 2.5 (n • 10), 25 (n • 10), and 250 (n • 10) ng of compound 48/80 for 30 min. ••, p • 0.01, and •, p • 0.05.

As shown in Fig. 2A, marked extravasation of Evans blue was seen in the ears of Ndrg1$^{-/-}$ mice 30 min after Ag challenge, whereas the ears of replicate Ndrg1$^{+/+}$ mice exhibited markedly less extravasation of the dye. Consistently, when tissue swelling of the left and right ears was measured with a dial thickness gauge, the change in ear thickness of Ndrg1$^{+/+}$ mice was as little as 40% compared with that of Ndrg1$^{-/-}$ mice (61.7 • 6.7 vs 24.7 • 4.3 • m in Ndrg1$^{+/+}$ and Ndrg1$^{-/-}$ mice, respectively; p • 0.01, n • 15) (Fig. 2B). To evaluate the extravasation of Evans blue quantitatively, the ears were removed and the OD of the extracted dye was measured as a function of Ag dose (Fig. 2C) or time (Fig. 2D). We observed that Evans blue extravasation was lower in Ndrg1$^{-/-}$ mice than in replicate Ndrg1$^{+/+}$ mice at all Ag doses (Fig. 2C) and all time points (Fig. 2D), even though dye extravasation was still evident in Ndrg1$^{-/-}$ mice. Furthermore, when these mice were intradermally administered compound 48/80, a polycationic IgE-independent mast cell secretogogue, a result similar to the IgE-associated passive immune response was obtained. Thus, the extravasation of Evans blue was only modest in Ndrg1$^{-/-}$ mice treated with compound 48/80 relative to that in replicate Ndrg1$^{+/+}$ mice (Fig. 2E). In mast cell-deficient W/W^v mice there was minimal dye extravasation under all conditions tested (Fig. 2, B–E). Collectively, these results indicate that NDRG1 deficiency causes a significant reduction of mast cell-associated passive systemic and local cutaneous anaphylactic reactions.

Histochemical and functional analyses of mast cells in Ndrg1-deficient mice

Because NDRG1 is widely expressed in many tissues/cells, it was still not apparent whether the diminished anaphylaxis reactions

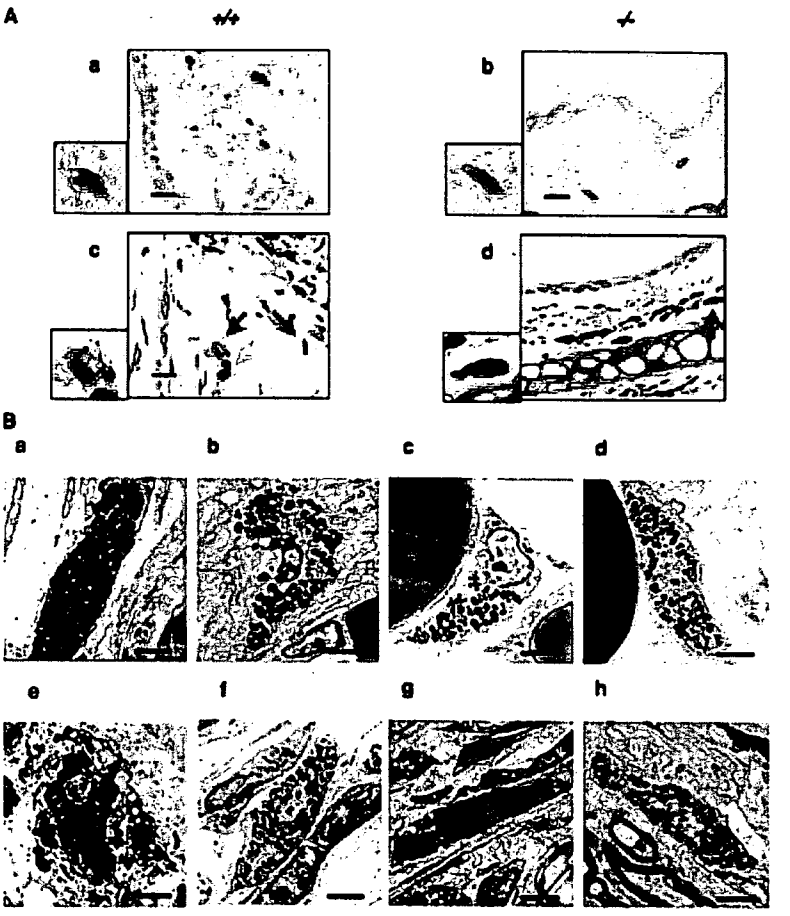

FIGURE 3. Histological and ultrastructural features of mast cells in the ear skin of wild-type and Ndrg1-deficient mice before and after Ag challenge. A, Ndrg1$^{+/+}$ (+/+) and Ndrg1$^{-/-}$ (-/-) mice were subjected to IgE-mediated, Ag-dependent PCA as described in Materials and Methods. Before and 2 min after Ag challenge the ear sections were stained with toluidine blue and examined by light microscopy. Photographs of Ndrg1$^{+/+}$ (a and c) and Ndrg1$^{-/-}$ (b and d) tissue sections before (a and b; n = 20 for each) and after (c and d; n = 10 for each) Ag challenge are shown. Yellow and red arrows indicate intact and degranulated tissue mast cells, respectively. Black arrows indicate chromocytes. Magnified views of a single mast cell for each are shown in the insets (a–d). Bar, 10 μm. B, Transmission electron microscopy (lead citrate staining) of ear skin mast cells in Ndrg1$^{+/+}$ (a, b, and e) and Ndrg1$^{-/-}$ (c, d, and f–h) mice before (a–d) and after (e–h) Ag challenge. Bar, 2 μm.

could be due to a defect in mast cells or other cell types, such as endothelial cells (39). To investigate the underlying mechanism(s) responsible for the reduced allergic reactions in Ndrg1-deficient mice, we next examined mast cells in the ear skin of wild-type and Ndrg1-deficient mice histochemically during the IgE-mediated, Ag-dependent PCA. Ear sections of Ndrg1$^{+/+}$ and Ndrg1$^{-/-}$ mice with or without Ag challenge were stained with toluidine blue to quantify degranulated tissue mast cells by light microscopy. In the absence of Ag challenge (no stimulation), the ear skin of Ndrg1$^{-/-}$ mice contained 37.8% fewer intact toluidine blue-positive mast cells than that of Ndrg1$^{+/+}$ mice (Fig. 3A, a and b, and Table I). After challenge with Ag for 2 min, the ear skin sections of Ndrg1$^{+/+}$ and Ndrg1$^{-/-}$ mice contained 18.8 and 2.8% degranulated mast cells relative to their respective total mast cells, revealing ~ 85% less degranulation in the null mice than in the control mice (Fig. 3A, c and d, and Table I). These observations suggest that the number of ear skin mast cells is reduced and that the degranulation efficacy of these cells is markedly impaired as a result of NDRG1 deficiency.

Table I. Quantification of ear skin mast cells in Ndrg1$^{+/+}$ and Ndrg1$^{-/-}$ mice[a]

	IgE/Ag	Intact	Degranulated
Ndrg1$^{+/+}$	No stimulation	660.7 ± 52.7	9.7 ± 2.0 (1.5%)
	Two minutes	930.0 ± 76.7	175.0 ± 10.8 (18.8%)
Ndrg1$^{-/-}$	No stimulation	411.3 ± 39.3*	4.4 ± 4.6* (1.0%)
	Two minutes	720.0 ± 50.4*	20.0 ± 6.6* (2.8%)

[a] Activation of skin mast cells (per mm^2) with or without Ag application was evaluated by counting the numbers of intact and degranulated toluidine blue-positive cells in 20 different ear sections from Ndrg1$^{+/+}$ (n = 5) and Ndrg1$^{-/-}$ (n = 5) mice by light microscopy. The results are expressed as mean ± SEM.

*, $p < 0.01$ vs Ndrg1$^{+/+}$ mice under each condition; percentages of degranulated mast cells relative to total mast cells are shown in parentheses.

To further corroborate the abnormal histochemical aspects of ear skin mast cells, we next examined their ultrastructural features by transmission electron microscopy after 2 min of stimulation with Ag in comparison with those of unstimulated cells. As shown in Fig. 3B, there were obvious and significant differences in secretory granule and cell surface morphology between Ndrg1$^{+/+}$ and Ndrg1$^{-/-}$ ear mast cells. Intact mast cells in Ndrg1$^{+/+}$ mice were oval with regular short processes and had many secretory granules filled with electron-lucent and dense contents (Fig. 3B, a and b). Relative to the mast cells in Ndrg1$^{+/+}$ mice, those in Ndrg1$^{-/-}$ mice had unusual granules that were small and irregular in size (Fig. 3B, c and d), suggesting immaturity. Two minutes after antigenic challenge the ear skin mast cells in Ndrg1$^{+/+}$ mice possessed swollen granules that exhibited a loss of crystalline materials and decreased electron density (Fig. 3Be). The fusion of swollen granules had resulted in the formation of large vacuolar degranulation channels continuous with the plasma membrane and, thereby, the appearance of large surface pores. Massive exocytosis, demonstrated by the extrusion of flocculent matrix materials through the surface pores into the extracellular space, was regularly observed in Ndrg1$^{+/+}$ mast cells (Fig. 3Be). In contrast, these Ag-induced morphological changes were scarcely observed in Ndrg1$^{-/-}$ mast cells (Fig. 3B, f, g, and h). Thus, it is likely that the reduced PCA response in Ndrg1-deficient mice (Fig. 2) resulted from abnormalities in the maturation and exocytosis of mast cells in the ear skin.

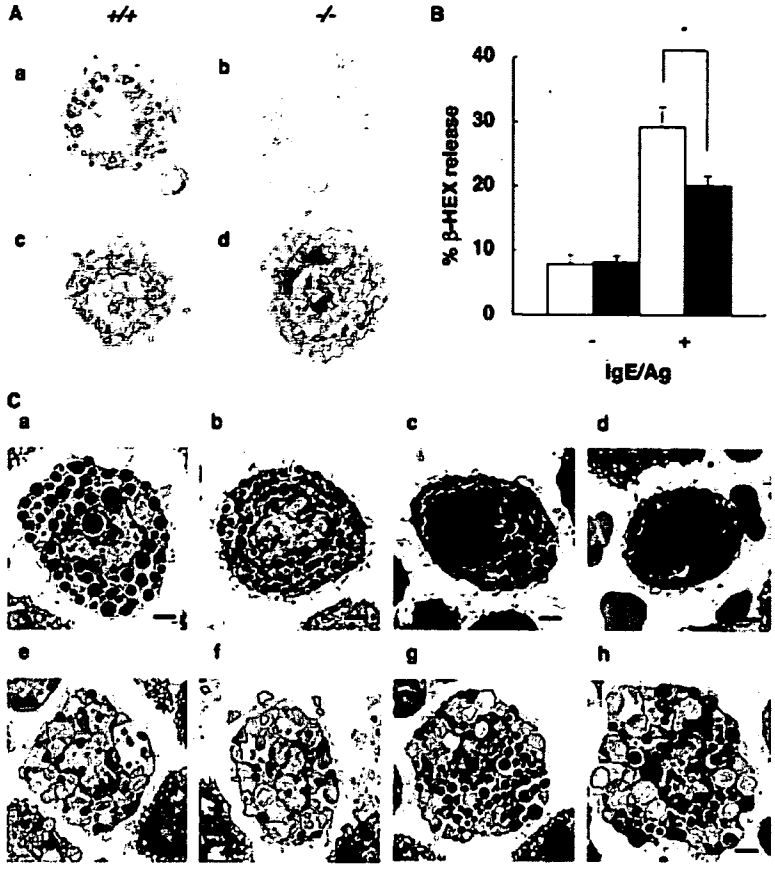

FIGURE 4. Morphology and exocytotic response of PMCs from wild-type and Ndrg1-deficient mice. A, Immunohistochemistry of NDRG1 in PMCs from Ndrg1$^{+/+}$ (a, • /•) and Ndrg1$^{-/-}$ (b, • /•) mice. In each case the cells were incubated with an anti-NDRG1 Ab and then with a HRP-conjugated anti-goat Ig. Other sets of PMC preparations from Ndrg1$^{+/+}$ (c) and Ndrg1$^{-/-}$ (d) mice were stained with safranin O. Representative data from five independent experiments are shown. B, The exocytotic response was determined by measuring the release of •-HEX. PMCs (10^6) from Ndrg1$^{+/+}$ (open bars) and Ndrg1$^{-/-}$ (filled bars) mice were sensitized with anti-DNP IgE and stimulated with DNP-BSA plus lyso-PS as described in Materials and Methods. •-HEX enzymatic activity (n • 6) was measured in supernatants and cell pellets solubilized with 0.5% Triton-X-100 in PIPES-buffered saline. •, p • 0.01. C, Transmission electron microscopy of PMCs prepared from Ndrg1$^{+/+}$ (a, b, e, and f) and Ndrg1$^{-/-}$ (c, d, g, and h) mice before (a–d) and after (e–h) exo vivo stimulation. Bar, 1 • m.

We then examined the morphology and ex vivo function of PMCs isolated from wild-type and Ndrg1-deficient mice. The immunostaining of cytospun PMCs with the anti-NDRG1 Ab showed intense immunoreactivity in Ndrg1$^{+/+}$ but not Ndrg1$^{-/-}$ PMCs (Fig. 4A, a and b), confirming the specificity of the Ab. Interestingly, NDRG1 immunoreactivity in Ndrg1$^{+/+}$ PMCs was largely associated with compact granular structures (Fig. 4Aa), a staining pattern similar to that of replicate cells treated with safranin O (Fig. 4Ac), which stains heparin-containing serglycin proteoglycan in secretory granules. Considering that NDRG1 is a cytosolic protein, this result may indicate that NDRG1 is located in close contact with the cytosolic surface of secretory granules. The fact that the granules in Ndrg1$^{+/+}$ and Ndrg1$^{-/-}$ PMCs were equally safranin-positive (Fig. 4A, c and d) suggests that NDRG1 deficiency does not affect heparin synthesis. Notably, safranin staining of cytospin preparations of peritoneal cells demonstrated that Ndrg1$^{-/-}$ mice contained 53.4% fewer safranin-positive PMCs than Ndrg1$^{+/+}$ mice (4885 • 492 vs 2280 • 225 per 10^6 peritoneal cells in Ndrg1$^{+/+}$ and Ndrg1$^{-/-}$ mice, respectively (p • 0.01), in 15 independent cytospin preparations). Hence, Ndrg1-deficient mice contain significantly less CTMC-type mast cells (both in the ear (Fig. 3) and the peritoneum (Fig. 4)) than do wild-type mice. We then compared IgE/Ag-dependent degranulation of PMCs from Ndrg1$^{+/+}$ and Ndrg1$^{-/-}$ mice by measuring the release level of the extracellular activity of •-HEX, a marker enzyme for histamine-containing granules. Because IgE/Ag-dependent activation of rodent PMCs is greatly augmented by lyso-PS (40–42), PMCs sensitized with anti-DNP IgE were stimulated by Fc•RI cross-linking with DNP-BSA as an Ag in the presence of lyso-PS as a cofactor. As shown in Fig. 4B, PMCs from Ndrg1$^{-/-}$ mice displayed significantly less release of •-HEX than those from Ndrg1$^{+/+}$ mice in response to IgE/Ag plus lyso-PS, whereas the basal release levels of these mediators were indistinguishable between the two genotypes.

Ultrastructural analyses under electron microscopy revealed that Ndrg1$^{-/-}$ mice contained a population of PMCs that looked similar to Ndrg1$^{+/+}$ PMCs (Fig. 4C, a and b for Ndrg1$^{+/+}$ and c for Ndrg1$^{-/-}$) and another population with fewer and irregular granules (Fig. 4Cd). After IgE/Ag (plus lyso-PS) stimulation, Ndrg1$^{-/-}$ PMCs were well degranulated (Fig. 4C, e and f), whereas a large portion of intact granules still remained in Ndrg1$^{-/-}$ PMCs (Fig. 4C, g and h). Thus, these functional and morphological studies imply that NDRG1 deficiency causes a reduced Fc•RI-mediated exocytotic response of CTMCs both in vivo (skin mast cells; Fig. 3) and ex vivo (PMCs; Fig. 4).

To further assess the differences in secretory granules between Ndrg1$^{+/+}$ and Ndrg1$^{-/-}$ mast cells, we measured the content of histamine and the activity of mast cell-associated proteases in homogenates of ears or peritoneal cells from both genotypes. Histamine levels and chymase-, typtase-, and CPA-like protease activities were pretty low in the ears (Fig. 5, Aa and B, a–c) and peritoneal cells (Fig. 5Ab) of mast cell-deficient W/W^v mice, confirming that mast cells are the main source of these granule components. As shown in Fig. 5A, histamine levels in the ears (a) and peritoneal cells (b) of Ndrg1$^{+/+}$ and Ndrg1$^{-/-}$ mice were comparable. Given that the number of mast cells was decreased by half in both ears and peritoneal cavities by Ndrg1 deficiency (see above), histamine content per PMC was estimated to nearly double in Ndrg1$^{-/-}$ over Ndrg1$^{+/+}$ mice (Fig. 5A, c and d). Measurement of chymase-like (Fig. 5Ba), tryptase-like (Fig. 5Bb), and CPA (Fig. 5Bc) activities in the ears showed that the tryptase-like, but not chymase-like and CPA, activity was significantly reduced in

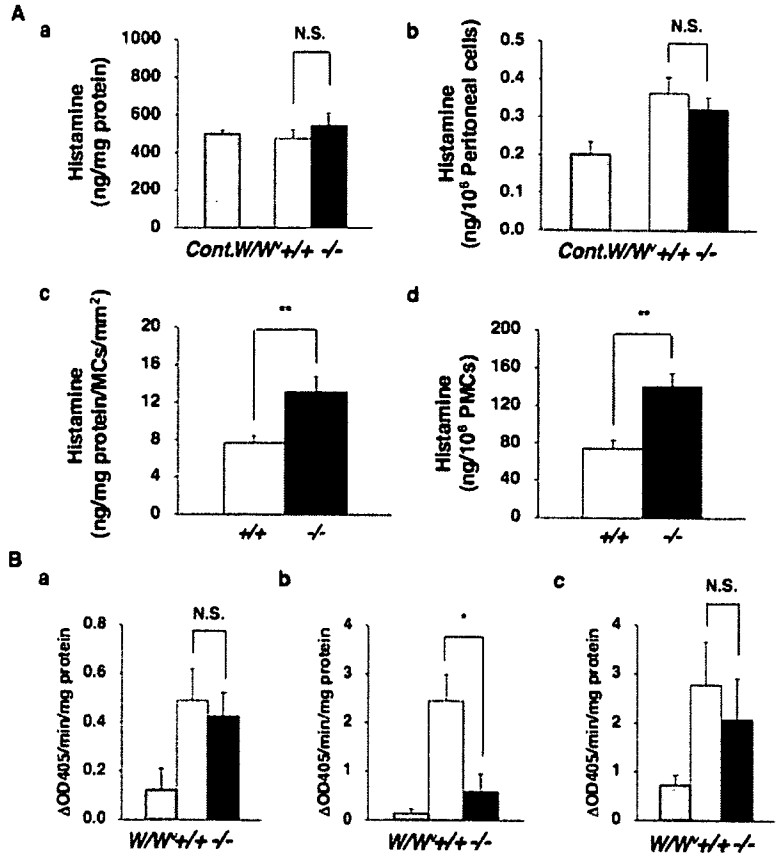

FIGURE 5. The storage of granule histamine and proteases in tissue mast cells of wild-type and Ndrg1-deficient mice. A, The histamine contents in ear extracts (a and c) and peritoneal cells (b and d) from Ndrg1$^{+/+}$ ($+/+$, n • 13), Ndrg1$^{-/-}$ ($-/-$, n • 12), control WBB6F$_1$-$+/+$ (Cont.W, n • 3), and WBB6F$_1$-W/W^v (W^v, n • 3) mice. Data were shown as histamine (ng) per protein of ear tissue (a) or 10^6 peritoneal cells (b) and per protein of ear skin mast cells per mm^2 (c) or 10^6 PMCs (d). ••, p • 0.01; and N.S., not significant. B, Protease activities in ear tissue extracts from Ndrg1$^{+/+}$ (n • 7), Ndrg1$^{-/-}$ (n • 8), and W/W^v (n • 5) mice. The extracts prepared from ear tissue were assayed for trypsin-like (a), chymotrypsin-like (b), and CPA (c) activities as described in Materials and Methods. Data were shown as protease activities per protein of ear tissue. •, p • 0.05; and N.S., not significant.

Ndrg1$^{-/-}$ mice compared with that in Ndrg1$^{+/+}$ mice. These results suggest that the absence of Ndrg1 alters the features of secretory granules in CTMCs.

Impaired maturation and reduced exocytotic degranulation of BMMCs derived from Ndrg1-deficient mice

To further evaluate the abnormal aspects of mast cells observed in Ndrg1-deficient mice, we analyzed BMMCs of Ndrg1$^{+/+}$ and Ndrg1$^{-/-}$ mice that were obtained after bone marrow cells were cultured for 4–5 wk in IL-3-containing medium. Nearly 95% of the cells in these cultures from both genotypes were mast cells, as they contained metachromatic granules after staining with Alcian blue (Fig. 6A, a and e) or toluidine blue (data not shown). The kinetics of cell growth and the expression of mast cell surface markers (c-kit$^+$ CD34$^+$ or c-kit$^+$ Sca-1$^+$ as determined by flow cytometric analysis) were also similar between the BMMCs from both sources (data not shown). Electron microscopy studies of various preparations of BMMCs from Ndrg1$^{+/+}$ and Ndrg1$^{-/-}$ mice revealed similar cell morphology and membrane projections and the presence of morphologically distinct cytoplasmic granules, including those with internal vacuoles (type I), those with an electron-dense core surrounded by membrane vacuoles (type II), and those completely filled with the electron-dense core (type III) (Fig. 6A, c and g) (43). These results indicate that NDRG1 is not essential for IL-3-dependent development of BMMCs from bone marrow progenitor cells.

We next examined whether the loss of NDRG1 would have some impact on the maturation of immature BMMCs toward CTMC-like mast cells. As reported previously, a coculture of BMMCs with Swiss 3T3 fibroblasts in the presence of SCF facilitates morphological and functional maturation toward a CTMC-like phenotype (14), and NDRG1 is an early inducible protein in this process (15). Therefore, as expected, NDRG1 protein was minimally expressed before coculture and was markedly induced after coculture in Ndrg1$^{+/+}$ BMMCs, whereas it was undetectable in Ndrg1$^{-/-}$ BMMCs irrespective of coculture (Fig. 6B). When Ndrg1$^{+/+}$ and Ndrg1$^{-/-}$ BMMCs after coculture with fibroblasts were counterstained with safranin O, the latter appeared less granulated than the former (Fig. 6A, b and f). Indeed, electron microscopy showed that, in contrast with cocultured Ndrg1$^{+/+}$ BMMCs in which type III secretory granules were well organized (Fig. 6Ad), replicate Ndrg1$^{-/-}$ BMMCs had mainly type I and type II secretory granules that were small and irregular in size and were partially unfilled with electron-lucent and dense contents (Fig. 6Ah). Moreover, the number of Ndrg1$^{+/+}$ BMMCs increased • 3-fold after 4 days of coculture, whereas replicate Ndrg1$^{-/-}$ BMMCs grew slower (2.9 • 0.2 vs 2.2 • 0.1 -fold for Ndrg1$^{+/+}$ and Ndrg1$^{-/-}$ BMMCs, respectively; p • 0.01; n • 13), suggesting that Ndrg1 deficiency has a propensity to reduce the expansion of mast cells interacting with fibroblasts.

We next performed RT-PCR using RNA samples from BMMCs of Ndrg1$^{+/+}$ and Ndrg1$^{-/-}$ mice to compare the expression patterns of all NDRG members. Consistent with our previous report (15), NDRG1 mRNA was weakly expressed before coculture and was highly induced as early as 1 h after the start of coculture in wild-type BMMCs, whereas it was not detected at all in Ndrg1-deficient BMMCs (Fig. 6C). We found that NDRG2, NDRG3, and NDRG4 mRNAs were also expressed in both Ndrg1$^{+/+}$ and Ndrg1$^{-/-}$ BMMCs (Fig. 6C). In contrast to the marked inducibility of NDRG1, expressions of NDRG2, NDRG3, and NDRG4 were nearly constant throughout the experimental period. Judging from the optimized PCR cycles, the expression level of NDRG1 was • 30-fold higher than that of NDRG3 and

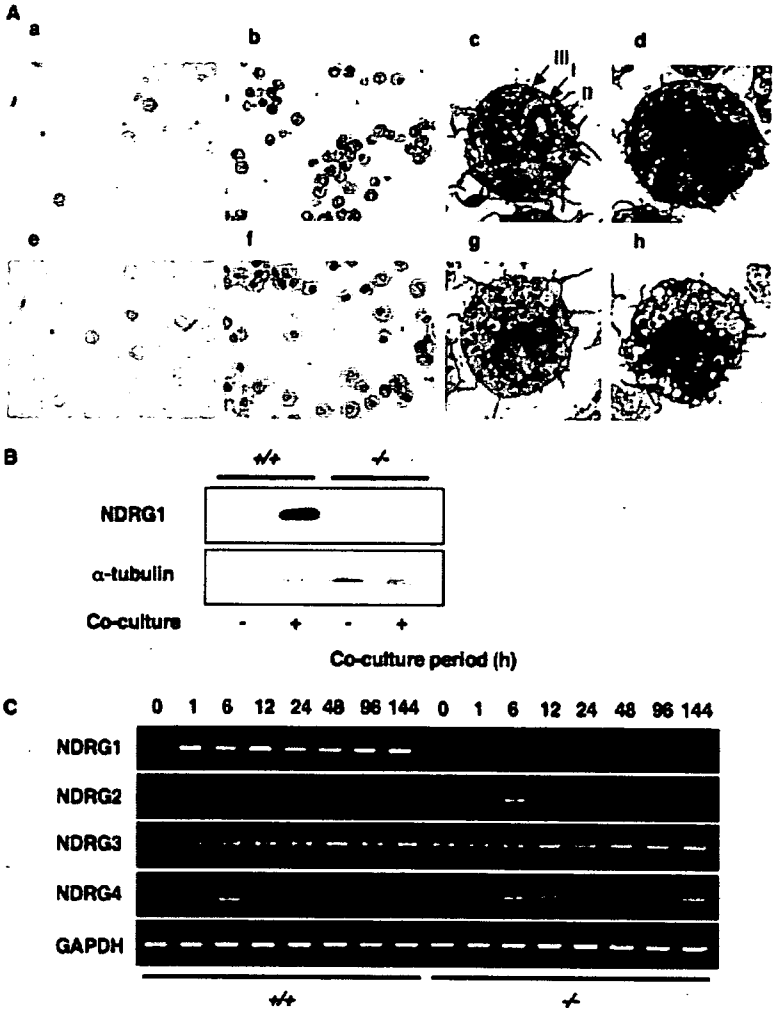

FIGURE 6. Histological and ultrastructural features of wild-type and Ndrg1-deficient BMMCs before and after coculture with fibroblasts. A, The cytospin preparations of Ndrg1$^{+/+}$ (a and b) and Ndrg1$^{-/-}$ (e and f) BMMCs before (a and e) and after (b and f) coculture with fibroblasts in the presence of SCF were stained by Alcian blue and safranin O. Ndrg1$^{+/+}$ (c and d) and Ndrg1$^{-/-}$ (g and h) BMMCs before (c and g) and after (d and h) coculture with fibroblasts were further analyzed by electron microscopy to reveal their ultrastructures. Typical types I, II, and III granules in BMMCs are shown by arrows. B, Expression of NDRG1 protein in Ndrg1$^{+/+}$ (+/+) and Ndrg1$^{-/-}$ (-/-) BMMCs before and after coculture with fibroblasts as assessed by Western blotting with anti-NDRG1 Ab. Blotting with β-tubulin was also performed to confirm the equal sample loading. Representative results for BMMCs from Ndrg1$^{+/+}$ and Ndrg1$^{-/-}$ mice are shown. C, mRNA expression of NDRG family members. RT-PCR analysis was performed on total RNA samples from Ndrg1$^{+/+}$ and Ndrg1$^{-/-}$ BMMCs before and after coculture for the indicated periods to detect transcripts for NDRG1 (23 cycles of amplification), NDRG2 (32 cycles), NDRG3 (28 cycles), and NDRG4 (35 cycles). Expression of GAPDH was examined as an internal control (23 cycles).

even more than that of NDRG2 and NDRG4 in wild-type BMMCs after coculture.

Next, we compared the granule release from Ndrg1$^{+/+}$ and Ndrg1$^{-/-}$ BMMCs before and after coculture with fibroblasts by measuring the extracellular activity of β-HEX. BMMCs were incubated with DNP-specific IgE and subsequently stimulated by FcεRI cross-linking with DNP-BSA. In dose-related (Fig. 7, A and C) and kinetic (Fig. 7, B and D) granule release responses, Ndrg1$^{-/-}$ BMMCs after coculture displayed significantly less exocytosis than did replicate Ndrg1$^{+/+}$ BMMCs (Fig. 7, C and D), whereas the responses of IL-3-maintained immature BMMCs derived from both genotypes were comparable (Fig. 7, A and B). It was noteworthy that Ndrg1$^{-/-}$ BMMCs after coculture released more β-HEX than before coculture, whereas this increased exocytosis after coculture was almost absent from Ndrg1$^{+/+}$ BMMCs. The total amount of β-HEX per cell did not differ between Ndrg1$^{+/+}$ and Ndrg1$^{-/-}$ BMMCs before and after coculture, and treatment with IgE alone did not induce granule release from either genotype (data not shown).

Because the coculture of BMMCs with fibroblasts led to the acquisition of responsiveness to compound 48/80 (14), we next compared the responses of Ndrg1$^{+/+}$ and Ndrg1$^{-/-}$ BMMCs to this G_i-coupled polycationic secretagogue after coculture with fibroblasts. The stimulation of cocultured Ndrg1$^{+/+}$ BMMCs with compound 48/80 resulted in marked exocytosis, whereas that of replicate Ndrg1$^{+/+}$ BMMCs provided partial albeit significant (~ 50% reduction as compared with Ndrg1$^{+/+}$ BMMCs) responses at all doses (Fig. 7E) and times (Fig. 7F) tested. Furthermore, β-HEX release in response to the Ca^{2+} ionophore (ionomycin) was also substantially reduced in Ndrg1$^{-/-}$ BMMCs relative to Ndrg1$^{+/+}$ BMMCs after coculture (61.0 and 41.7% release in Ndrg1$^{+/+}$ and Ndrg1$^{-/-}$ BMMCs, respectively, at 1 μM ionomycin). Collectively, these observations suggest that Ndrg1-deficient BMMCs after coculture with fibroblasts in the presence of SCF are functionally less mature than replicate wild-type BMMCs.

To gain further insights into the attenuated exocytotic response of Ndrg1$^{-/-}$ BMMCs after coculture with fibroblasts, we next examined several parameters of mast cell activation following FcεRI signaling. When the expression of mast cell surface markers in Ndrg1$^{+/+}$ and Ndrg1$^{-/-}$ BMMCs before coculture was monitored by flow cytometric analysis, markers of BMMCs, including c-kit (Fig. 8A, a and b) and IgE-bound FcεRI (Fig. 8A, e and f) were equally expressed in cells of both genotypes. After coculture with fibroblasts, Ndrg1$^{+/+}$ and Ndrg1$^{-/-}$ BMMCs still expressed similar levels of c-kit (Fig. 8A, c and d). Remarkably, the expression of FcεRI was elevated in cocultured Ndrg1$^{-/-}$ BMMCs (Fig. 8Ag), whereas this increase was negligible in replicate Ndrg1$^{+/+}$ BMMCs (Fig. 8Ah). Accordingly, Ndrg1$^{-/-}$ BMMCs expressed a lower level of FcεRI than did Ndrg1$^{+/+}$ BMMCs after coculture (Fig. 8A, f and h). Tyrosine phosphorylation of the β isoforms of PLC, which hydrolyze phosphatidylinositol bisphosphate to

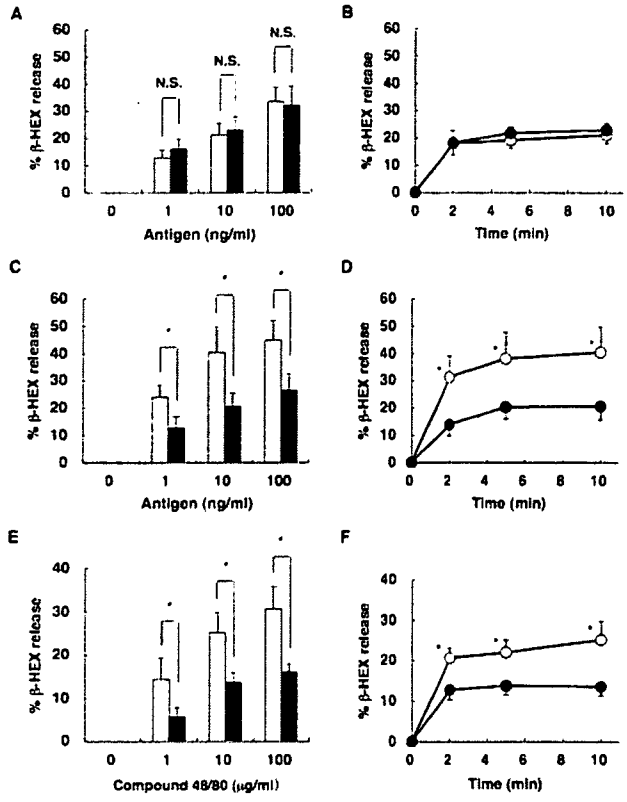

FIGURE 7. The exocytotic response of wild-type and Ndrg1-deficient BMMCs before and after coculture with fibroblasts as assessed by release of •-HEX. Ndrg1$^{+/+}$ (• /• , open symbols) and Ndrg1$^{-/-}$ (• /• , filled symbols) BMMCs before (A and B) and after (C and D) coculture with fibroblasts were preloaded with anti-DNP IgE and stimulated with the indicated concentrations of DNP-BSA (A and C) and with 10 ng/ml DNP-BSA for the indicated periods (B and D). Alternatively, Ndrg1$^{+/+}$ and Ndrg1$^{-/-}$ BMMCs after coculture with fibroblasts were stimulated with the indicated concentrations of compound 48/80 (E) and 10 • g/ml compound 48/80 for the indicated periods (F). Data shown are the mean • SEM of at least six independent experiments with triplicate samples at each point. •, p • 0.05; and ••, p • 0.01 vs Ndrg1$^{+/+}$ BMMCs.

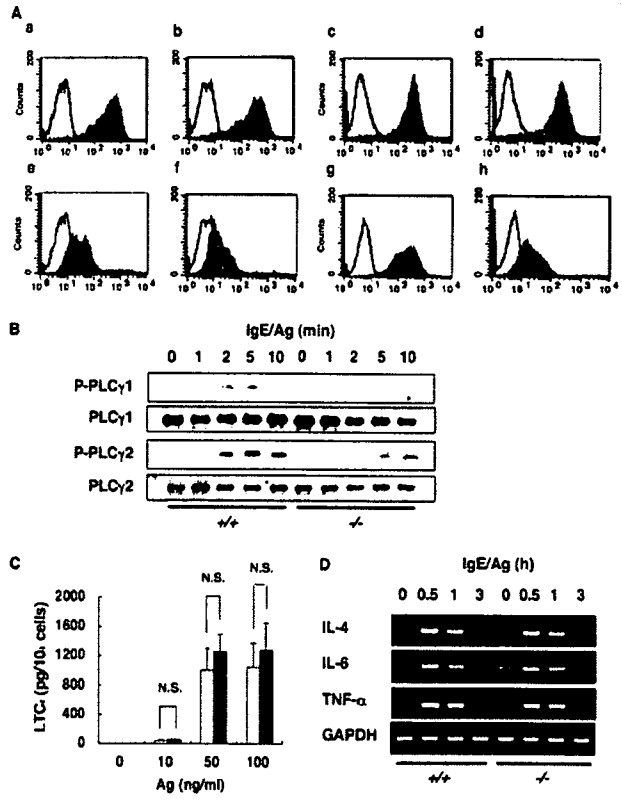

FIGURE 8. Fc•RI signaling of wild-type and Ndrg1-deficient BMMCs after coculture with fibroblasts. A, Surface expression of c-kit and Fc•RI in BMMCs before and after coculture with fibroblasts. Ndrg1$^{+/+}$ (a, c, e, and g) and Ndrg1$^{-/-}$ (b, d, f, and h) BMMCs before (a, b, e, and f) and after (c, d, g, and h) coculture with fibroblasts were incubated with or without 10 • g/ml mouse IgE, and then stained with PE-labeled anti-mouse IgE Ab (e–h). c-kit expression was detected with FITC-labeled anti-mouse c-Kit Ab (a–d). Representative histograms of BMMCs from three independent experiments are shown. B, Tyrosine phosphorylation of PLC•1 or PLC•2 in BMMCs after coculture with fibroblasts. IgE-sensitized BMMCs from Ndrg1$^{+/+}$ (• /•) and Ndrg1$^{-/-}$ (• /•) mice were stimulated with DNP-BSA for indicated times. Lysates from these cells were subjected SDS-PAGE, transferred to nitrocellulose membrane filters, and then immunoblotted with Abs against tyrosine-phosphorylated forms of PLC•1 and PLC•2 (P-PLC•1 and P-PLC•2, respectively). After stripping, the filters were reprobed with anti-PLC•1 or anti-PLC•2 Ab to determine their protein levels. C, LTC_4 production by Ndrg1$^{+/+}$ (open bars) and Ndrg1$^{-/-}$ (filled bars) BMMCs after coculture with fibroblasts. The IgE-sensitized cells were stimulated with the indicated doses of Ab for 30 min. LTC_4 levels in the supernatants were measured by ELISA. N.S., not significant. D, Expression of cytokine mRNAs in BMMCs after coculture with fibroblasts. Total RNAs were extracted from cocultured Ndrg1$^{+/+}$ and Ndrg1$^{-/-}$ following stimulation for the indicated periods with IgE and Ag and then subjected to RT-PCR for IL-4 (30 cycles), IL-6 (25 cycles), and TNF-• (25 cycles) as well as GAPDH (control; 23 cycles) using the respective specific primers.

produce the second messengers inositol triphosphate and diacylglycerol, is an early post-Fc•RI event that is subsequently linked to intracellular Ca^{2+} mobilization and protein kinase C activation (44–46). As shown in Fig. 8B, the phosphorylation of PLC•1 and PLC•2, which occurred within a few minutes after Ag challenge as revealed by immunoblotting with Abs specific for phosphorylated PLC• isoforms, was partially reduced in cocultured Ndrg1$^{-/-}$ BMMCs compared with replicate wild-type BMMCs, although the total amount of each PLC• isoform was indistinguishable between the both genotypes. These results raised the possibility that the reduced Fc•RI-mediated exocytotic response in cocultured Ndrg1$^{-/-}$ BMMCs (Fig. 7) might be at least partly attributable to a defective maturation-associated elevation of Fc•RI expression (Fig. 8A) and, thereby, reduced activation of PLC• (Fig. 8B).

However, the production of cysteinyl LTC_4, an arachidonate-metabolizing product, which depends entirely on an increased intracellular Ca^{2+} level and MAPK (47, 48), was unaffected in Ndrg1$^{-/-}$ BMMCs after coculture (Fig. 8C). In addition, Fc•RI-induced expression of several cytokines including IL-4, IL-6 and TNF-•, an event that depends on the activation of multiple signaling pathways such as protein kinase C, MAPK, NF-•B, NF-AT, or PI3K (49–54), occurred normally in Ndrg1$^{-/-}$ BMMCs even after coculture (Fig. 8D). Consistently, the increase in intracellular Ca^{2+}, an upstream event for LT and cytokine generation after Fc•RI cross-linking, was comparable between cocultured Ndrg1$^{+/+}$ and Ndrg1$^{-/-}$ BMMCs (data not shown). These results argue that the residual activation of PLC• is still sufficient for downstream signaling pathways, leading to full eicosanoid synthesis and cytokine expression in cocultured Ndrg1$^{-/-}$ BMMCs. It appears, therefore, that the reduced degranulation in Ndrg1$^{-/-}$ BMMCs may have resulted from a regulatory step(s) other than the receptor-proximal events.

Discussion

Recent reports that overexpression or knockdown of NDRG1 in cultured neoplastic cells alters their proliferation, differentiation, metastasis, and apoptosis statuses (25, 28, 29, 55–58) and that genetic mutations in the Ndrg1 gene cause Schwann cell dysfunction leading to peripheral neuropathy in both human and mouse (30–32) imply that this inducible intracellular protein plays roles in diverse processes linked to these cellular events. Despite its widespread distribution, however, the regulatory expression and functions of NDRG1, particularly in the immune system, have been poorly understood. We previously found that NDRG1 is markedly induced during ex vivo differentiation of IL-3-dependent BMMCs, a relatively immature population of mast cells, into more mature CTMC-like cells that contain safranin-positive secretory granules, produce large amounts of PGD_2, and show sensitivity to G protein-coupled polycationic secretagogues such as compound 48/80 and substance P (14, 15). Although the forcible transfection of NDRG1 into a mast cell-line augmented the exocytotic response (15), an event suggesting the potential ability of this protein to promote the functional maturation of mast cells, the physiological relevance of these observations has still remained elusive. In an effort to gain further insight into the functional roles of NDRG1 in mast cell biology, in the present study we examined mast cell-associated phenotypes of Ndrg1-deficent mice. Our results provided evidence that NDRG1 plays a pivotal role in the terminal maturation and effector function (degranulation) of mast cells in vivo and ex vivo.

Ndrg1$^{*/*}$ mice were partially resistant to passive systemic anaphylaxis, displaying only modest changes in rectal temperature and plasma histamine level in comparison with the replicate Ndrg1$^{*/*}$ littermate control (Fig. 1). Likewise, in the passive cutaneous anaphylactic response Ndrg1$^{*/*}$ mice exhibited attenuated extravasation (an event triggered by mast cell-derived mediators such as histamine and cysteinyl LTs) at the sites of stimuli (Fig. 2), whereas skin mast cells in the null mice showed only minimal degranulation (Fig. 3). The latter observation is supported by the ex vivo experiments showing that PMCs from Ndrg1$^{*/*}$ mice were less sensitive to Fc•RI cross-linking than those from Ndrg1$^{*/*}$ mice (Fig. 4B). In addition to these functional defects, dermal and serosal CTMCs of Ndrg1$^{*/*}$ mice contained fewer and unusual secretory granules (Figs. 3–5), suggesting their immaturity.

Studies using the culture system in which BMMCs differentiate into CTMC-like cells revealed that, although immature BMMCs maintained in IL-3 were virtually identical between the Ndrg1$^{*/*}$ and Ndrg1$^{*/*}$ genotypes, after maturation into CTMC-like cells by coculture with fibroblasts in the presence of SCF the BMMCs showed several notable differences in terms of ultrastructure and function. Thus, as compared with the Ndrg1$^{*/*}$ control, Ndrg1$^{*/*}$ BMMCs after coculture contained aberrant secretory granules that were small and irregular with a paucity of electron-lucent and dense contents (Fig. 6), in agreement with the altered morphology of dermal and serosal CTMCs in Ndrg1$^{*/*}$ mice as mentioned above (Figs. 3–5). In addition, the retarded proliferation of Ndrg1$^{*/*}$ BMMCs in coculture may be a reflection of reduced mast cell number in vivo. The coculture was accompanied by augmented Fc•RI-mediated exocytosis in Ndrg1$^{*/*}$ BMMCs, whereas this event did not occur appreciably in replicate Ndrg1$^{*/*}$ BMMCs (Fig. 7). The surface expression levels of c-kit, CD34, and Sca-1 on BMMCs were similar between the two genotypes irrespective of coculture, indicating that NDRG1 does not affect the expression of these early mast cell surface markers (data not shown). Interestingly, the expression of Fc•RI was elevated in Ndrg1$^{*/*}$ but not in Ndrg1$^{*/*}$ BMMCs after coculture (Fig. 8A), and this change appears to be associated with reduced PLC• phosphorylation, an Fc•RI-proximal event, in Ndrg1$^{*/*}$ BMMCs (Fig. 8B). However, almost normal LT synthesis and cytokine expression in cocultured Ndrg1$^{*/*}$ BMMCs (Fig. 8, C and D) argues against the contribution of the moderate changes in these receptor-proximal events to the reduced exocytosis. It is also notable that the exocytotic response to compound 48/80, a G_i-coupled secretagogue to which response became apparent after coculture, as well as the response to ionomycin, a Ca^{2+} ionophore, was also partially reduced in cocultured Ndrg1$^{*/*}$ BMMCs compared with replicate Ndrg1$^{*/*}$ cells (Fig. 7, E and F). These results are in agreement with our previous observation that the overexpression of NDRG1 in RBL-2H3 mastocytoma led to a marked enhancement of degranulation but not eicosanoid synthesis following various stimuli (15). Thus, it is speculated that NDRG1 plays a role in the divergent signaling at the point of convergence or beyond leading to exocytosis.

Whereas it has been reported that NDRG1 shows cytoplasmic, nuclear, and even mitochondrial localization and often shuttles between the cytoplasm and the nucleus according to cell type, stimulus, and cell cycle stage (15, 25, 39, 59, 60), in the present study we found that in mast cells NDRG1 exhibits a unique punctate distribution in the cytoplasm, particularly around secretory granules (Fig. 4). A likely explanation for this location is that NDRG1 binds to certain proteins or lipid components that are enriched in the mast cell granule membranes. Interestingly, by means of yeast two-hybrid screening we and others have recently found that NDRG1 has the potential capacity to associate with several cellular proteins, such as HSC70, PICK-1, p47, Pra1, RTN-1C, and Aip-1, all of which are known to participate in cellular events related to membrane transport and fusion (59, 60). The interrelated protein trafficking of NDRG1 binding partners points to its possible involvement in the complex network of vesicular transport. In relation to this, the blood level of high-density lipoprotein is reduced in CMT4D patients harboring the R148X mutation in the Ndrg1 gene (60), and several genetic disorders of lipid vesicular transport cause the CMT-like peripheral neuropathy that accompanies demyelination (61, 62). These facts raise the possibility that the neuropathic phenotype of Ndrg1 mutation might be due to a perturbation of lipid trafficking and membrane transport in Schwann cells. Moreover, high steady-state expression of NDRG1 is found in renal proximal tubular and intestinal epithelial cells, which actively transport vesicles with polarity from apical to basolateral membranes (39). Thus, apart from the regulatory role of NDRG1 in the terminal maturation of mast cells, the reduced exocytosis of Ndrg1-null mast cells may be indicative of an additional role of this protein in the regulation of the secretory process. Supporting this idea, our recent GeneChip analysis of Ndrg1$^{*/*}$ vs Ndrg1$^{*/*}$ BMMCs after coculture has revealed that Ndrg1 deficiency leads to a marked reduction in the expression of a panel of genes related to cytoskeletal organization and rearrangement (data not shown) that could have a deep impact on cellular shape, cell division, membrane integrity and fusion, vesicular transport, and even exocytotic function. A possible functional link of NDRG1 with each component of those GeneChip-identified genes is now under investigation at molecular levels.

The finding that there are fewer electron-dense secretory granules in CTMCs in Ndrg1$^{*/*}$ mice than in Ndrg1$^{*/*}$ mice is suggestive of substantial changes in the granule contents. Because • 50% of the weight of a PMC consists of protease/proteoglycan complexes that are packaged in the cell granules, we evaluated for

gross changes in total protease levels by using colorimetric substrates and found that tryptase-like activity was markedly diminished in Ndrg1* /* PMCs compared with littermate control PMCs (Fig. 5B). In contrast, the chymase-like and CPA activities, as well as heparin content as judged from safranin-positive staining (Figs. 4A and 6A) and N-deacetylase/N-sulfotransferase-2 expression (data not shown), appeared to be unaffected by the absence of NDRG1. Because transcripts for the four major CTMC-associated proteases, mMCP-4, mMCP-5, mMCP-6, and mMC-CPA3, did not differ significantly between Ndrg1* /* and Ndrg1* /* mice (data not shown), selective reduction of the tryptase-like activity in Ndrg1* /* mice might be caused at posttranslational rather than transcriptional levels. Unexpectedly, Ndrg1* /* CTMCs contained more histamine than did Ndrg1* /* CTMCs (Fig. 5A, c and d). We speculate that the reduction in physiological histamine secretion from CTMCs upon microenvironmental stimuli in Ndrg1* /* mice might eventually result in the accumulated storage of granule histamine. Nevertheless, although the regulation of individual granule components by NDRG1 needs further elucidation, at this stage we can say that NDRG1 deficiency influences several if not all granule materials, possibly as a result of the alterations in granule moiety and heterogeneity.

Although the molecular mechanisms whereby NDRG1 regulates several processes in mast cells (and possibly in other cell types) are still a subject of debate, it is intriguing to note that the NDRG1 protein has several intriguing motifs, including the phosphopantetheine-binding site, the esterase/lipase/thioesterase domain, and the three Ser/Thr-rich tandem repeats, which might be responsible for protein-protein interaction, subcellular localization, and posttranslational modification such as phosphorylation. We have recently shown that deletion of the C-terminal Ser/Thr-rich repeats abrogates the degranulation-enhancing potential of NDRG1 (15) and that NDRG1 undergoes phosphorylation of Ser and Thr residues in mast cells (63). Interestingly, a recent study has shown that Ser/Thr-rich repeats provide sites for the sequential phosphorylation by serum- and glucocorticoid-induced kinase 1 (SGK1) and then by glycogen synthase kinase 3 (GSK3) (64, 65). Thus, SGK1/GSK3-directed phosphorylation within these repeats might constitute a regulatory pathway for NDRG1-mediated signals.

In summary, this study is the first to demonstrate that Ndrg1 deficiency profoundly affects the terminal maturation and a particular effector function (degranulation), thereby affecting mast cell-associated pathological outcomes, i.e., anaphylactic responses. Unexplained is why Ndrg1* /* BMMCs before coculture already have a normal degranulation response. In this regard, it is possible that other NDRG members (NDRG2–4) that are constitutively expressed in BMMCs regardless of the coculture (Fig. 6C) might play a redundant role. Nonetheless, it is important to clarify the relevance of this study to human mast cell development and associated diseases. Interestingly, human mast cells express NDRG1 as well as NDRG2 as evidenced by Affymetrix GeneChip transcript data (66). We have also confirmed in our preliminary study that human cord blood-derived mast cells also express NDRG1 (data not shown), although the proper culture condition under which NDRG1 expression could be modified in these cells has not yet been defined. Determining the regulatory expression and function of NDRG1 (as well as other NDRG members) in human mast cells would shed further light on the importance of this family of proteins in the context of the pathology of allergy and other mast cell-associated biological events. Moreover, continued analyses of Ndrg1-null mice in combination with ongoing GeneChip analysis will expand our understanding of the unexplored roles of this unique protein in the homeostasis and disorders of the mast cell-related and -unrelated immune systems as well as in other pathogenic events including neuronal degeneration and cancer.

Acknowledgment

We thank Dr. Atsushi Iwama (Laboratory of Stem Cell Therapy, Center for Experimental Medicine, Tokyo, Japan) for help with flow cytometric analyses.

Disclosures

The authors have no financial conflict of interest.

References

1. Kitamura, Y., M. Yokoyama, H. Matsuda, T. Ohno, and K. J. Mori. 1981. Spleen colony-forming cell as common precursor for tissue mast cells and granulocytes. Nature 291: 159–160.
2. Nakahata, T., S. S. Spicer, J. R. Cantey, and M. Ogawa. 1982. Clonal assay of mouse mast cell colonies in methylcellulose culture. Blood 60: 352–361.
3. Metcalfe, D. D., D. Baram, and Y. A. Mekori. 1997. Mast cells. Physiol. Rev. 77: 1033–1079.
4. Galli, S. J., M. Tsai, and C. S. Lantz. 1999. The regulation of mast cell and basophil development by the kit ligand, SCF, and IL-3. In Signal Transduction in Mast Cells and Basophils. E. Razin and J. Rivera, eds. Springer-Verlag, New York, pp. 11–30.
5. Kitamura, Y., E. Morii, and T. Jippo. 1999. The c-kit receptor and the mi transcription factor: two important molecules for mast cell development. In Signal Transduction in Mast Cells and Basophils. E. Razin and J. Rivera, eds. Springer-Verlag, New York, pp. 31–38.
6. Wong, G. W., D. S. Friend, and R. L. Stevens. 1999. Mouse and rat models of mast cell development. In Signal Transduction in Mast Cells and Basophils. E. Razin, and J. Rivera, eds. Springer-Verlag, New York, pp. 39–53.
7. Huang, E., K. Nocka, D. R. Beier, T. Y. Chu, J. Buck, H. W. Lahm, D. Wellner, P. Leder, and P. Besmer. 1990. The hematopoietic growth factor KL is encoded by the Sl locus and is the ligand of the c-kit receptor, the gene product of the W locus. Cell 63: 225–233.
8. Nocka, K., J. Buck, E. Levi, and P. Besmer. 1990. Candidate ligand for the c-kit transmembrane kinase receptor: KL, a fibroblast derived growth factor stimulates mast cells and erythroid progenitors. EMBO J. 9: 3287–3294.
9. Gurish, M. F., H. Tao, J. P. Abonia, A. Arya, D. S. Friend, C. M. Parker, and K. F. Austen. 2001. Intestinal mast cell progenitors require CD49d•7 (•4•7 integrin) for tissue-specific homing. J. Exp. Med. 194: 1243–1252.
10. Abonia, J. P., K. F. Austen, B. J. Rollins, S. K. Joshi, R. A. Flavell, W. A. Kuziel, P. A. Koni, and M. F. Gurish. 2005. Constitutive homing of mast cell progenitors to the intestine depends on autologous expression of the chemokine receptor CXCR2. Blood 105: 4308–4313.
11. Levi-Schaffer, F., K. F. Austen, P. M. Gravallese, and R. L. Stevens. 1986. Coculture of interleukin 3-dependent mouse mast cells with fibroblasts results in a phenotypic change of the mast cells. Proc. Natl. Acad. Sci. USA 83: 6485–6488.
12. Levi-Schaffer, F., E. T. Dayton, K. F. Austen, A. Hein, J. P. Caulfield, P. M. Gravallese, F. T. Liu, and R. L. Stevens. 1987. Mouse bone marrow-derived mast cells cocultured with fibroblasts: morphology and stimulation-induced release of histamine, leukotriene B_4, leukotriene C_4, and prostaglandin D_2. J. Immunol. 139: 3431–3441.
13. Dayton, E. T., P. Pharr, M. Ogawa, W. E. Serafin, K. F. Austen, F. Levi-Schaffer, and R. L. Stevens. 1988. 3T3 fibroblasts induce cloned interleukin 3-dependent mouse mast cells to resemble connective tissue mast cells in granular constituency. Proc. Natl. Acad. Sci. USA 85: 569–572.
14. Ogasawara, T., M. Murakami, T. Suzuki-Nishimura, M. K. Uchida, and I. Kudo. 1997. Mouse bone marrow-derived mast cells undergo exocytosis, prostanoid generation, and cytokine expression in response to G protein-activating polybasic compounds after coculture with fibroblasts in the presence of c-kit ligand. J. Immunol. 158: 393–404.
15. Taketomi, Y., T. Sugiki, T. Saito, S. Ishii, M. Hisada, T. Suzuki-Nishimura, M. K. Uchida, T. C. Moon, H. W. Chang, Y. Natori, et al. 2003. Identification of NDRG1 as an early inducible gene during in vitro maturation of cultured mast cells. Biochem. Biophys. Res. Commun. 306: 339–346.
16. Kikuchi-Yanoshita, R., Y. Taketomi, K. Koga, T. Sugiki, Y. Atsumi, T. Saito, S. Ishii, M. Hisada, T. Suzuki-Nishimura, M. K. Uchida, et al. 2003. Induction of PYPAF1 during in vitro maturation of mouse mast cells. J. Biochem. 134: 699–709.
17. Shaw, E., L. A. McCue, C. E. Lawrence, and J. S. Dordick. 2002. Identification of a novel class in the •/• hydrolase fold superfamily: the N-myc differentiation-related proteins. Proteins 47: 163–168.
18. Okuda, T., and H. Kondoh. 1999. Identification of new genes Ndr2 and Ndr3 which are related to Ndr1/RTP/Drg1 but show distinct tissue specificity and response to N-myc. Biochem. Biophys. Res. Commun. 266: 208–215.
19. Zhou, R. H., K. Kokame, Y. Tsukamoto, C. Yutani, H. Kato, and T. Miyata. 2001. Characterization of the human NDRG gene family: a newly identified member, NDRG4, is specifically expressed in brain and heart. Genomics 73: 86–97.
20. Qu, X., Y. Zhai, H. Wei, C. Zhang, G. Xing, Y. Yu, and F. He. 2002. Characterization and expression of three novel differentiation-related genes belong to the human NDRG gene family. Mol. Cell. Biochem. 229: 35–44.

21. Kokame, K., H. Kato, and T. Miyata. 1996. Homocysteine-respondent genes in vascular endothelial cells identified by differential display analysis. GRP78/BiP and novel genes. J. Biol. Chem. 271: 29659–29665.
22. Lin, T. M., and C. Chang. 1997. Cloning and characterization of TDD5, an androgen target gene that is differentially repressed by testosterone and dihydrotestosterone. Proc. Natl. Acad. Sci. USA 94: 4988–4993.
23. van Belzen, N., W. N. Dinjens, M. P. Diesveld, N. A. Groen, A. C. van der Made, Y. Nozawa, R. Vlietstra, J. Trapman, and F. T. Bosman. 1997. A novel gene which is up-regulated during colon epithelial cell differentiation and down-regulated in colorectal neoplasms. Lab. Invest. 77: 85–92.
24. Zhou, D., K. Salnikow, and M. Costa. 1998. Cap43, a novel gene specifically induced by Ni^{2+} compounds. Cancer Res. 58: 2182–2189.
25. Kurdistani, S. K., P. Arizti, C. L. Reimer, M. M. Sugrue, S. A. Aaronson, and S. W. Lee. 1998. Inhibition of tumor cell growth by RTP/rit42 and its responsiveness to p53 and DNA damage. Cancer Res. 58: 4439–4444.
26. Shimono, A., T. Okuda, and H. Kondoh. 1999. N-myc-dependent repression of Ndr1, a gene identified by direct subtraction of whole mouse embryo cDNAs between wild type and N-myc mutant. Mech. Dev. 83: 39–52.
27. Park, H., M. A. Adams, P. Lachat, F. Bosman, S. C. Pang, and C. H. Graham. 2000. Hypoxia induces the expression of a 43-kDa protein (PROXY-1) in normal and malignant cells. Biochem. Biophys. Res. Commun. 276: 321–328.
28. Guan, R. J., H. L. Ford, Y. Fu, Y. Li, L. M. Shaw, and A. B. Pardee. 2000. Drg-1 as a differentiation-related, putative metastatic suppressor gene in human colon cancer. Cancer Res. 60: 749–755.
29. Bandyopadhyay, S., S. K. Pai, S. C. Gross, S. Hirota, S. Hosobe, K. Miura, K. Saito, T. Commes, S. Hayashi, M. Watabe, and K. Watabe. 2003. The Drg-1 gene suppresses tumor metastasis in prostate cancer. Cancer Res. 63: 1731–1736.
30. Kalaydjieva, L., D. Gresham, R. Gooding, L. Heather, F. Baas, R. de Jonge, K. Blechschmidt, D. Angelicheva, D. Chandler, P. Worsley, et al. 2000. N-myc downstream-regulated gene 1 is mutated in hereditary motor and sensory neuropathy-Lom. Am. J. Hum. Genet. 67: 47–58.
31. Hunter, M., R. Bernard, E. Freitas, A. Boyer, B. Morar, I. J. Martins, I. Tournev, A. Jordanova, V. Guergelcheva, B. Ishpekova, et al. 2003. Mutation screening of the N-myc downstream-regulated gene 1 (NDRG1) in patients with Charcot-Marie-tooth disease. Hum. Mutat. 22: 129–135.
32. Okuda, T., Y. Higashi, K. Kokame, C. Tanaka, H. Kondoh, and T. Miyata. 2004. Ndrg1-deficient mice exhibit a progressive demyelinating disorder of peripheral nerves. Mol. Cell. Biol. 24: 3949–3956.
33. Pivniouk, V. I., T. R. Martin, J. M. Lu-Kuo, H. R. Katz, H. C. Oettgen, and R. S. Geha. 1999. SLP-76 deficiency impairs signaling via the high-affinity IgE receptor in mast cells. J. Clin. Invest. 103: 1737–1743.
34. Shore, P. A., A. Burkhalter, and V. H. Cohn, Jr. 1959. A method for the fluorometric assay of histamine in tissues. J. Pharmacol. Exp. Ther. 127: 182–186.
35. Nishizumi, H., and T. Yamamoto. 1997. Impaired tyrosine phosphorylation and Ca^{2+} mobilization, but not degranulation, in Lyn-deficient bone marrow-derived mast cells. J. Immunol. 158: 2350–2355.
36. Tchougounova, E., G. Pejler, and M. Abrink. 2003. The chymase, mouse mast cell protease 4, constitudes the major chymotrypsin-like activity in peritoneum and ear tissue: a role for mouse mast cell protease 4 in thrombin regulation and fibronectin turnover. J. Exp. Med. 198: 423–431.
37. Olenchock, B. A., R. Guo, M. A. Silverman, J. N. Wu, J. H. Carpenter, G. A. Koretzky, and X. P. Zhong. 2006. Impaired degranulation but enhanced cytokine production after Fc•RI stimulation of diacylglycerol kinase •-deficient mast cells. J. Exp. Med. 203: 1471–1480.
38. Dombrowicz, D., V. Flamand, K. K. Brigman, B. H. Koller, and J. P. Kinet. 1993. Abolition of anaphylaxis by targeted disruption of the high affinity immunoglobulin E receptor • chain gene. Cell 75: 969–796.
39. Lachat, P., P. Shaw, S. Gebhard, N. van Belzen, P. Chaubert, and F. T. Bosman. 2002. Expression of NDRG1, a differentiation-related gene, in human tissues. Histochem. Cell Biol. 118: 399–408.
40. Martin, T. W., and D. Lagunoff. 1979. Interactions of lysophospholipids and mast cells. Nature 279: 250–252.
41. Murakami, M., I. Kudo, Y. Fujimori, H. Suga, and K. Inoue. 1991. Group II phospholipase A_2 inhibitors suppressed lysophosphatidylserine-dependent degranulation of rat peritoneal mast cells. Biochem. Biophys. Res. Commun. 181: 714–721.
42. Hosono, H., J. Aoki, Y. Nagai, K. Bandoh, M. Ishida, R. Taguchi, H. Arai, and K. Inoue. 2001. Phosphatidylserine-specific phospholipase A_1 stimulates histamine release from rat peritoneal mast cells through production of 2-acyl-1-lysophosphatidylserine. J. Biol. Chem. 276: 29664–29970.
43. Raposo, G., D. Tenza, S. Mecheri, R. Peronet, C. Bonnerot, and C. Desaymard. 1997. Accumulation of major histocompatibility complex class II molecules in mast cell secretory granules and their release upon degranulation. Mol. Biol. Cell 8: 2631–2645.
44. Saitoh, S., R. Arudchandran, T. S. Manetz, W. Zhang, C. L. Sommers, P. E. Love, J. Rivera, and L. E. Samelson. 2000. LAT is essential for Fc•RI-mediated mast cell activation. Immunity 12: 525–535.
45. Gu, H., K. Saito, L. D. Klaman, J. Shen, T. Fleming, Y. Wang, J. C. Pratt, G. Lin, B. Lim, J. P. Kinet, and B. G. Neel. 2001. Essential role for Gab2 in the allergic response. Nature 12: 186–190.
46. Wen, R., S. T. Jou, Y. Chen, A. Hoffmeyer, and D. Wang. 2002. Phospholipase C•2 is essential for specific function of Fc•R and Fc•R. J. Immunol. 169: 6743–6752.
47. Chang, W. C., and A. B. Parekh. 2004. Close functional coupling between Ca^{2+} release-activated Ca^{2+} channels, arachidonic acid release, and leukotriene C_4 secretion. J. Biol. Chem. 279: 29994–29999.
48. Chang, W. C., C. Nelson, and A. B. Parekh. 2006. Ca^{2+} influx through CRAC channels activates cytosolic phospholipase A_2, leukotriene C_4 secretion, and expression of c-fos through ERK-dependent and -independent pathways in mast cells. FASEB J. 20: 2381–2383.
49. Nechushtan, H., M. Leitges, C. Cohen, G. Kay, and E. Razin. 2000. Inhibition of degranulation and interleukin-6 production in mast cells derived from mice deficient in protein kinase C•. Blood 95: 1752–1757.
50. Garrington, T. P., T. Ishizuka, P. J. Papst, K. Chayama, S. Webb, T. Yujiri, W. Sun, S. Sather, D. M. Russell, S. B. Gibson, et al. 2000. MEKK2 gene disruption causes loss of cytokine production in response to IgE and c-Kit ligand stimulation of ES cell-derived mast cells. EMBO J. 19: 5387–5395.
51. Peng, Y., M. R. Power, B. Li, and T. J. Lin. 2005. Inhibition of IKK down-regulates antigen • IgE-induced TNF production by mast cells: a role for the IKK-IB-NF-B pathway in IgE-dependent mast cell activation. J. Leukocyte Biol. 77: 975–983.
52. Kitaura, J., K. Asai, M. Maeda-Yamamoto, Y. Kawakami, U. Kikkawa, and T. Kawakami. 2000. Akt-dependent cytokine production in mast cells. J. Exp. Med. 192: 729–740.
53. Klein, M., S. Klein-Hessling, A. Palmetshofer, E. Serfling, C. Tertilt, T. Bopp, V. Heib, M. Becker, C. Taube, H. Schild, et al. 2006. Specific and redundant roles for NFAT transcription factors in the expression of mast cell-derived cytokines. J. Immunol. 177: 6667–6674.
54. Fukao, T., T. Yamada, M. Tanabe, Y. Terauchi, T. Ota, T. Takayama, T. Asano, T. Takeuchi, T. Kadowaki, J. Hata Ji, and S. Koyasu. 2002. Selective loss of gastrointestinal mast cells and impaired immunity in PI3K-deficient mice. Nat. Immunol. 3: 295–304.
55. Motwani, M., F. M. Sirotnak, Y. She, T. Commes, and G. K. Schwartz. 2002. Drg1, a novel target for modulating sensitivity to CPT-11 in colon cancer cells. Cancer Res. 62: 3950–3955.
56. Li, J., and L. Kretzner. 2003. The growth-inhibitory Ndrg1 gene is a Myc negative target in human neuroblastomas and other cell types with overexpressed N- or c-myc. Mol. Cell. Biochem. 250: 91–105.
57. Kim, K. T., P. P. Ongusaha, Y. K. Hong, S. K. Kurdistani, M. Nakamura, K. P. Lu, and S. W. Lee. 2004. Function of Drg1/Rit42 in p53-dependent mitotic spindle checkpoint. J. Biol. Chem. 279: 38597–38602.
58. Stein, S., E. K. Thomas, B. Herzog, M. D. Westfall, J. V. Rocheleau, R. S. Jackson II, M. Wang, and P. Liang. 2004. NDRG1 is necessary for p53-dependent apoptosis. J. Biol. Chem. 279: 48930–48940.
59. Sugiki, T., Y. Taketomi, R. Kikuchi-Yanoshita, M. Murakami, and I. Kudo. 2004. Association of N-myc downregulated gene 1 with heat-shock cognate protein 70 in mast cells. Biol. Pharm. Bull. 27: 628–633.
60. Hunter, M., D. Angelicheva, I. Tournev, E. Ingley, D. C. Chan, G. F. Watts, I. Kremensky, and L. Kalaydjieva. 2005. NDRG1 interacts with APO A-I and A-II and is a functional candidate for the HDL-C QTL on 8q24. Biochem. Biophys. Res. Commun. 332: 982–992.
61. Chance, P. F. 2004. Genetic evaluation of inherited motor/sensory neuropathy. Suppl. Clin. Neurophysiol. 57: 228–242.
62. Parman, Y., E. Battaloglu, I. Baris, B. Bilir, M. Poyraz, N. Bissar-Tadmouri, A. Williams, N. Ammar, E. Nelis, V. Timmerman, et al. 2004. Clinicopathological and genetic study of early-onset demyelinating neuropathy. Brain 127: 2540–2550.
63. Sugiki, T., M. Murakami, Y. Taketomi, R. Kikuchi-Yanoshita, and I. Kudo. 2004. N-myc downregulated gene 1 is a phosphorylated protein in mast cells. Biol. Pharm. Bull. 27: 624–627.
64. Murray, J. T., D. G. Campbell, N. Morrice, G. C. Auld, N. Shpiro, R. Marquez, M. Peggie, J. Bain, G. B. Bloomberg, F. Grahammer, et al. 2004. Exploitation of KESTREL to identify NDRG family members as physiological substrates for SGK1 and GSK3. Biochem. J. 384: 477–488.
65. Murray, J. T., L. A. Cummings, G. B. Bloomberg, and P. Cohen. 2005. Identification of different specificity requirements between SGK1 and PKB•. FEBS Lett. 579: 991–994.
66. Dahl, C., H. Saito, M. Kruhoffer, and P. O. Schiotz. 2006. Identification of tryptase- and chymase-related gene clusters in human mast cells using microarrays. Allergy 61: 276–280.